Characterizing Southeast Greenland fjord surface ice and freshwater flux to support biological applications

Twila A. Moon[1*], Benjamin Cohen[2*], Taryn E. Black[2,3], Kristin L. Laidre[2], Harry L. Stern[2], Ian Joughin[2]

[1]National Snow and Ice Data Center, Cooperative Institute for Research in Environmental Sciences, University of Colorado, Boulder, 80309, USA
[2]Polar Science Center, Applied Physics Laboratory, University of Washington, Seattle, 98105, USA
[3]Earth System Science Interdisciplinary Center, University of Maryland, College Park, MD 20742, USA
* These authors contributed equally to the work.

Correspondence to: Twila A. Moon (twila.moon@colorado.edu)

Short summary. *(500-character limit)*

The complex geomorphology of Southeast Greenland (SEG) creates dynamic fjord habitats for marine top predators, with glacier-derived floating ice, pack and landfast sea ice, and freshwater flux. We investigate the SEG fjord physical environment, with a focus on surface ice conditions, to provide a regional characterization to support biological research. As Arctic warming continues, SEG may serve as a long-term refugia for ice-dependent wildlife due to projected regional ice sheet persistence.

Abstract.

Southeast Greenland (SEG) is characterized by complex morphology and environmental processes that create dynamic habitats for resident marine top predators. Active glaciers producing solid ice discharge, freshwater flux, offshore sea ice transport, and seasonal landfast ice formation all contribute to a variable, transient environment within SEG fjord systems. Here, we investigate a selection of physical processes in SEG to provide a regional characterization to reveal physical system processes and support biological research. SEG fjords exhibit high fjord-to-fjord variability regarding bathymetry, size, shape, and glacial setting, influencing some processes more than others. For example, the timing of offshore sea ice formation in fall near SEG fjords progresses temporally southward across latitudes while the timing of offshore sea ice disappearance is less dependent on latitude. Rates of annual freshwater flux into fjords, in contrast, are highly variable across SEG, with annual average input values ranging from ~1×10^8 m^3 to ~1.25×10^{10} m^3 (~0.1–12.5 Gt) for individual fjords. Similarly, rates of solid ice discharge in SEG fjords vary widely – in part due to the irregular distribution of active glaciers across the study area (60°N-70°N). Landfast sea ice, assessed for 8 focus fjords, is seasonal and has a spatial distribution highly dependent on individual fjord topography. Conversely, glacial ice is deposited into fjord systems year-round, with the

spatial distribution of glacier-derived ice dependent on glacier termini location. As climate change continues to affect SEG, the evolution of these metrics will be individually variable in their response, and next steps should include moving from characterization to system projection. Due to projected regional ice sheet persistence that will continue to feed glacial ice into fjords, it is possible that SEG could remain a long-term (century to millennia scale) refugia location for polar bears and other ice-dependent species, demonstrating a need for continued research on the SEG physical environment.

1 Introduction and motivation

Rapid changes across the Greenland coastal environment are influencing the linked physical and biological fjord systems. The Greenland Ice Sheet and peripheral glaciers and ice caps are undergoing substantial retreat along marine- and land-terminating boundaries, revealing new ocean and terrestrial zones (Moon et al., 2020; Kochtitzky and Copland, 2022; Bosson et al., 2023). For some marine-terminating glaciers, changing ice dynamic and terminus locations are altering iceberg calving styles or rates (e.g., van Dongen et al., 2021), with potential influence on glacier-derived fjord ice that forms important habitat for polar bears *(Ursus maritimus),* seals, and many other marine species (e.g., Laidre et al., 2022). Increases in ice sheet surface melt are also changing the timing and quantity of subglacial meltwater discharge and terrestrial riverine freshwater input into the coastal fjords (e.g., van As et al., 2018). Depending on the fjord bathymetry and glacier grounding line depth, this subglacial discharge may entrain deeper nutrient-rich ocean water and assist in redistributing it to the surface photic zone to support enhanced primary productivity (Hopwood et al., 2018; Meire et al., 2023) or alter the ecosystem in other potentially significant ways (e.g., Murray et al., 2015; Holding et al., 2019; Sejr et al., 2022; Hopwood et al., 2020). Additional terrestrial runoff adds to coastal zone freshwater (e.g., from Norway: McGovern et al., 2020), though impacts are less well documented for Greenland (Meire et al., 2023). Despite the rapid physical changes underway, progress is still needed on fundamental physical characterization of the Greenland coastal zone, including the remote Southeast Greenland (SEG) region (Fig. 1).

Earlier work characterized the landfast sea ice (also referred to as fast ice) and glacier-derived fjord surface ice for five SEG fjords that were biologically relevant to polar bears (Laidre et al., 2022). This research revealed that glacier-derived fjord surface ice exists during time periods outside of the landfast sea ice season, and that this glacier-derived ice can act as an alternative habitat platform for marine species, allowing small populations to persist in areas they may not otherwise be able to. Surface ice presence may also alter other factors, such as light availability in the water column, salinity, or ocean water mixing, that may be of interest to other biological researchers. Motivated by the biological insight enabled via enhanced physical system knowledge, here we extend our characterization of the SEG fjord physical environment. Examining the full SEG region of interest (Fig. 1), we describe the freshwater flux, offshore sea ice, and solid glacier ice discharge behavior across the region during 2015 through 2019. We also expand from the five focus fjords used in Laidre et al. (2022) to eight focus fjords across SEG (Fig. 1, Table 1). For these focus fjords, we analyze landfast sea ice and glacier-derived ice presence
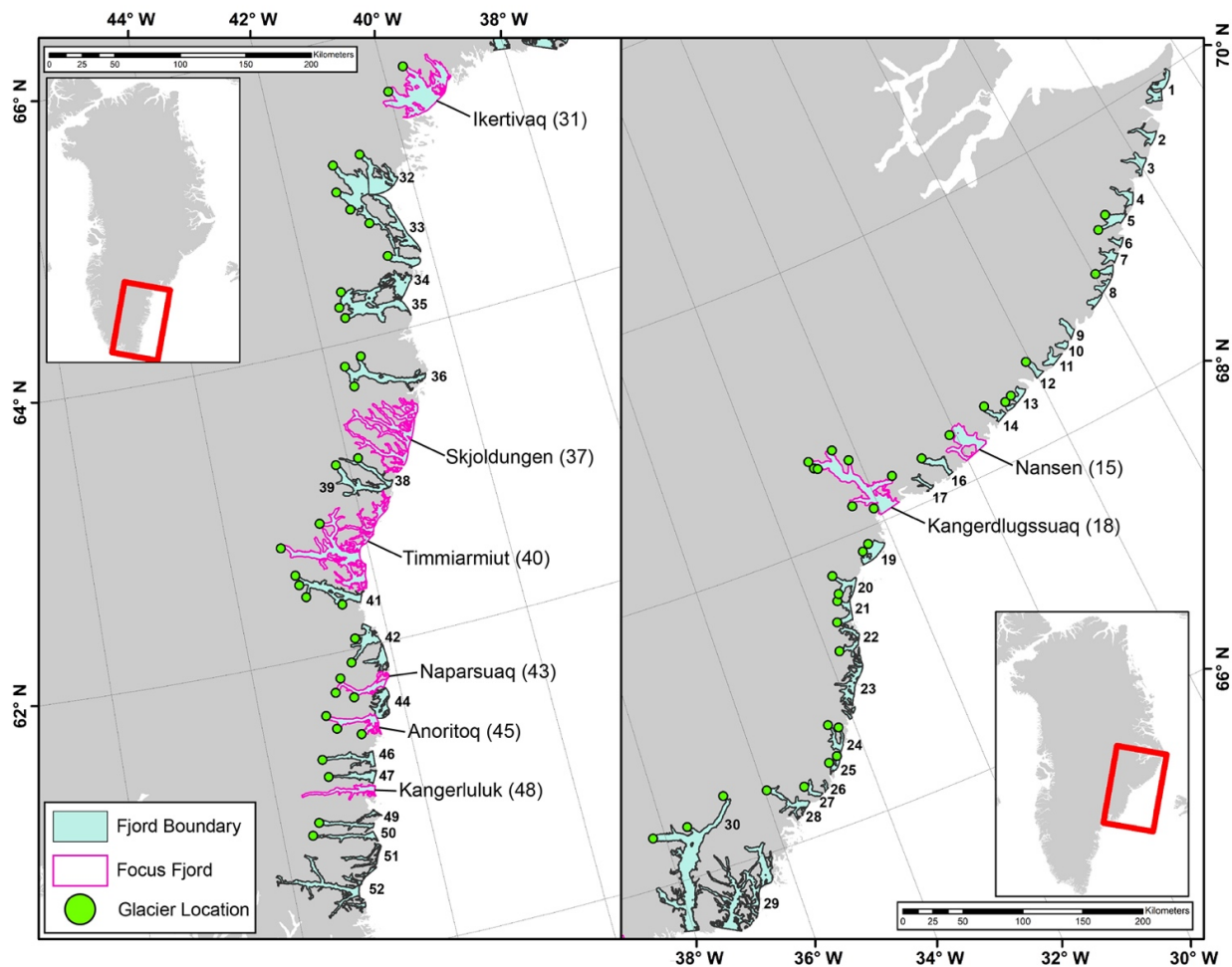
Figure 1. Southeast Greenland region of study, showing the 52 fjord systems defined across the full region (blue shading) and the 8 focus fjords used for fast ice and glacier-derived ice analysis (pink outlines). Locations of outlet glaciers considered in analysis of solid ice discharge are shown (green points).

63   in time and space and compare these results with offshore sea ice from satellite observations, and freshwater flux, sea surface

64   temperature, and sea ice cover from a regional climate model. Our results are designed to expand knowledge of SEG fjord

65   environments and pair with ongoing and future research into the linked physical and biological systems of the region.

66   **2 Southeast Greenland (SEG) study region**

67   While some fjords, for example Sermilik on the East Coast and Nuup Kangerlua (previously also known as Godthåbsfjord)

68   on the West Coast, have been studied more extensively, many Greenland fjords have proven difficult to study, including in

69   Southeast Greenland (SEG). Here, we define the SEG region of interest as extending from 60° N to 70° N (Fig. 1). This

70   region is of particular interest for a variety of reasons. First, it provides habitat for a genetically distinct polar bear

71   subpopulation only recently identified (Laidre et al., 2022). Second, it contains particularly remote regions of Greenland

72   coastline, far from any human settlements and difficult to access for research. Third, it is an area of very high winter

73   precipitation (Gallagher et al., 2021) and modeling work indicates that it may be one of the last regions of Greenland to

74   retain substantial coastal land ice (Aschwanden et al., 2019; Bochow et al., 2023). Fourth, it is a region of rapid change, not

75   only in documented changes to the coastal glaciers and ice sheet (Moon et al., 2020) but also notable declines in offshore sea

76   ice and warming of coastal ocean currents (Heide-Jørgensen et al., 2022).

3 Data and methods

78   In this study, the fjords in SEG are numbered 1-52 going from north to south (Fig. 1). We also use our own digitized fjord

79   boundaries created based on synthetic aperture radar (SAR) image mosaics (Cohen et al., 2023; see Code and data availability).

80   Our analysis is focused on 1 January 2015 through 31 December 2019 to align with SEG polar bear data collection and the

81   time period of interest established by Laidre et al. (2022).

82   To characterize a range of environmental metrics, we take advantage of existing data products, such as freshwater flux, solid

83   ice discharge, and regional climate model output, to create new datasets that support SEG-wide analysis. While remote sensing

84   is necessary to characterize a region of this scale, the spatial resolution needed (10s to 100s of meters) for some data types is

85   difficult to achieve from many standard remote sensing products, such as sea-ice cover data products (often with multi-

86   kilometer resolution). Though researchers are working towards automated classification schemes at the spatial scales needed

87   for this type of analysis (e.g., Scheick et al., 2019; Soldal et al. 2019), we are unaware of any that can support our specific

88   study needs. We therefore undertook extensive manual digitization to create landfast sea ice and glacier-derived fjord ice data

89   records. Along with supporting our analysis, these data (Cohen et al., 2023) should be helpful for ongoing work to improve

90   machine learning techniques for classifying fjord environments.

91   Due to the effort required to create manually digitized datasets, we selected eight focus fjords for landfast sea ice and glacier-

92   derived fjord ice analysis (Fig. 1, Table 1). Our focus fjords include five that were selected for Laidre et al. (2022): Skjoldungen

93   (63.3º N), Timmiarmiut (62.6º N), Naparsuaq (61.7º N), Anoritoq (61.5º N), and Kangerluluk (61.1º N). These fjords have

94   been occupied by polar bears for multiple years based on telemetry data collected since 2015 and comprised the core range of

95   the SEG polar bear population. Here, we expand the fjord selection to include three more northerly focus fjords: Ikertivaq

96   (65.4° N), Kangerdlugssuaq (68.1° N), and Nansen (68.2° N). Ikertivaq and Kangerdlugssuaq fjords are heavily used by polar

97   bears that inhabit Northeast Greenland, while their presence was scarcer in Nansen during 2015–2019. Skjoldungen (fjord 37)

98   and Kangerluluk (fjord 48) do not have glacier solid ice discharge that is included in our source dataset (see section 3.1), but

99   we include these fjords to allow us to analyze a wide range of fjord environments with varying levels of glacier-derived ice

100   input and polar bear use (which informed this research design) and we do digitize some glacier-derived ice in these two fjords

101 (see section 3.5). The map-view geometries of our focus fjords (Fig. 1) cover a wide range, from relatively simply shaped long,
102 narrow fjords (e.g., fjords 43 and 48) to complex interconnected channel systems (e.g., fjords 37 and 40).

Table 1. Focus fjord spatial information, including fjord reference names and numbers, areas (km²), and bounding coordinates used for analysis.

Fjord name & number	Analysis area (km²)	Top right (lat, lon)	Bottom left (lat, lon)
Nansen (15)	375	(68.43, -29.51)	(68.16, -30.32)
Kangerdlugssuaq (18)	880	(68.64, -31.52)	(68.05, -32.98)
Ikertivaq (31)	894	(65.74, -38.96)	(65.36, -40.13)
Skjoldungen (37)	793	(63.57, -40.80)	(63.08, -41.94)
Timmiarmiut (40)	1079	(62.98, -41.52)	(62.37, -43.22)
Naparsuaq (43)	182	(61.83, -42.11)	(61.68, -42.90)
Anoritoq (45)	217	(61.61, -42.40)	(61.41, -43.12)
Kangerluluk (48)	184	(61.12, -42.64)	(61.02, -43.64)

3.1 Solid ice discharge across SEG

104 To compute solid-ice discharge from 2015 through 2019, we used data derived from glacier gates (Mankoff et al., 2020b;
105 Mankoff et al., 2020c). These data were used to create individual glacier discharge time series as well as discharge by-fjord,
106 including daily, monthly, annual and season mean, and cumulative 2015-2019 discharge records (Cohen et al., 2023).
107 Beginning with a glacier dataset evolved from Moon et al. (2020), we manually associated each of these glaciers (shown in
108 Fig. 1) with a glacier gate in the Mankoff et al. (2020b) solid ice discharge dataset; in some cases, there were multiple gates
109 corresponding to a single glacier, and we summed the discharge from these gates accordingly. We filtered out data at times
110 when the dataset coverage attribute was less than 50% (Mankoff et al., 2020b). We also note that some glaciers apparent in
111 satellite imagery are not included in either the Moon et al. (2020) or Mankoff et al. (2020b) datasets (usually because they
112 are narrow and/or slow moving) and are therefore not included in our solid ice discharge results, even though glacier-derived
113 ice in fjords is recorded in a separate dataset (section 3.5). Solid ice discharge observation availability is visualized in Fig.
114 A1.

115 Solid ice discharge is interpolated for individual glaciers to create daily time series. We linearly interpolate between
116 observed discharge values to fill data gaps and use the observed discharge and error to calculate the interpolation error (Eqn
117 15, White, 2017). At the fjord level, the interpolated daily discharge time series for each glacier are summed together, and
118 the fjord discharge error is the root of the sum of the squares of the glacier discharge errors. The daily time series is then
119 used to construct other solid ice discharge metrics, including a monthly time series, as displayed in Fig. 9d.

120 To construct the daily time series, the ice discharge interpolation uses data from 180 days before and after our time period of
121 interest to ensure a complete daily record during our time period of interest. Two glaciers do not have data within these
122 pre/post-study periods (nor for several years prior), leading to a small discrepancy at the record edges since we are not able
123 to interpolate the records for periods without sufficient input data. In other words, the two glaciers were likely discharging,
124 but discharge observations were absent or filtered out for quality, and so the first or last several days in the interpolated time
125 series for those glaciers are empty. The resulting discrepancy between the cumulative discharge from all glaciers and the
126 cumulative discharge from all fjords is 3.8 Gt or 0.39%.

127 **3.2 Freshwater flux across SEG**

128 To compute daily time series of freshwater discharge into each fjord from 2015 through 2019, we used freshwater discharge
129 data, including surface runoff and subglacial discharge, from Greenland land and ice basins (Mankoff, 2020; Mankoff et al.,
130 2020a). We discuss freshwater as defined by these data, which partition regional climate model runoff estimates to ice and
131 coastal outlets. These freshwater flux data exclude contributions from evaporation, condensation, sea ice formation/melt,
132 subglacial basal melt, and precipitation directly onto the ocean surface. Small peripheral glaciers may also be excluded from
133 the regional climate model domain, though peripheral glaciers are scarce in our region of interest. Our freshwater flux
134 analysis also excludes in-fjord glacier-derived ice melt, which in some fjords may be a meaningful year-round source of
135 freshwater, particularly at the surface and within the ocean mixed layer (Enderlin et al., 2018; Moon et al. 2018). The
136 importance of in-fjord glacier-derived ice melt will be highly variable across SEG due to the large variation in glacier-
137 derived ice presence. For subglacial basal melt, omitted fluxes are dependent on the glacier basins that contribute to each
138 fjord (e.g., basin size, ice motion, subglacial hydrology). While the dataset presented here provides a step forward from
139 recently published freshwater flux values for marine-terminating glaciers only (Karlsson et al. 2023) by providing an
140 integrated fjord perspective and including fluxes from all ice sheet and terrestrial basins, it does not include subglacial basal
141 melt, which is available in Karlsson et al. (2023). Future work could create a regional or pan-Greenland dataset that includes
142 more freshwater flux sources and thus takes the next steps in providing a freshwater dataset without exclusions; for example,
143 including additions from subglacial melt analyzed across the ice sheet (Karlsson et al. 2021) or for marine-terminating
144 glaciers (Karlsson et al. 2023). Previous research suggests that pan-Greenland basal melt, driven by geothermal heat flux,
145 basal friction, and heat from transported surface meltwater, is 4.5% of annual solid ice discharge, but can be a much larger
146 contributor for marine-terminating glacier basins wherein these drivers are enhanced (Karlsson et al. 2021).

The freshwater discharge data products used and presented here are created by applying a flow routing algorithm to digital elevation models of the land and ice sheet surfaces and the ice sheet bed to identify land surface and subglacial streams, stream outlets, and basins upstream of those outlets. Subsequently, daily runoff from a regional climate model is summed over each of the identified basins, and instantaneously routed to the appropriate basin outlets. We calculated freshwater discharge into our fjords by using the command line tool provided with Mankoff et al. (2020a) to identify all outlets within a 500 m buffer of each fjord boundary; we applied this buffer to account for differences in coastline data products and to ensure that we captured all freshwater discharge outlets. We then used the command line tool to compute daily freshwater discharge originating from the predefined land and ice basins and going through the outlets that we identified and into each of our fjord basins. We used discharge values from the Modèle Atmosphérique Régional (MAR: Fettweis et al. 2017) and the Regional Atmospheric Climate Model (RACMO: Noël et al., 2019), both of which were statistically downscaled to a common 1 km grid and archived for use with these freshwater discharge tools (Mankoff, 2020); we used version 4.2 of the archival data. Due to a longer time series and to align with other sampled metrics, we relied primarily on the MAR time series, but we have included the RACMO discharge output in our own archival data.

160   We also analyzed freshwater discharge variations with depth, including terrestrial runoff and subglacial discharge. We used

161   the same command line interface and source data (Mankoff et al., 2020a) to identify all freshwater discharge outlets within

162   each buffered fjord boundaries. These outlet output data include outlet elevation above or below sea level. For outlets above

163   sea level, we clipped their elevation values to 0 m under the assumption that water flowing from these outlets enters the

164   fjords at sea level (i.e., surface runoff). Using these data, we calculated daily time series of total freshwater discharge, binned

165   by discharge depth, for each fjord (for example, Fig. 9c).
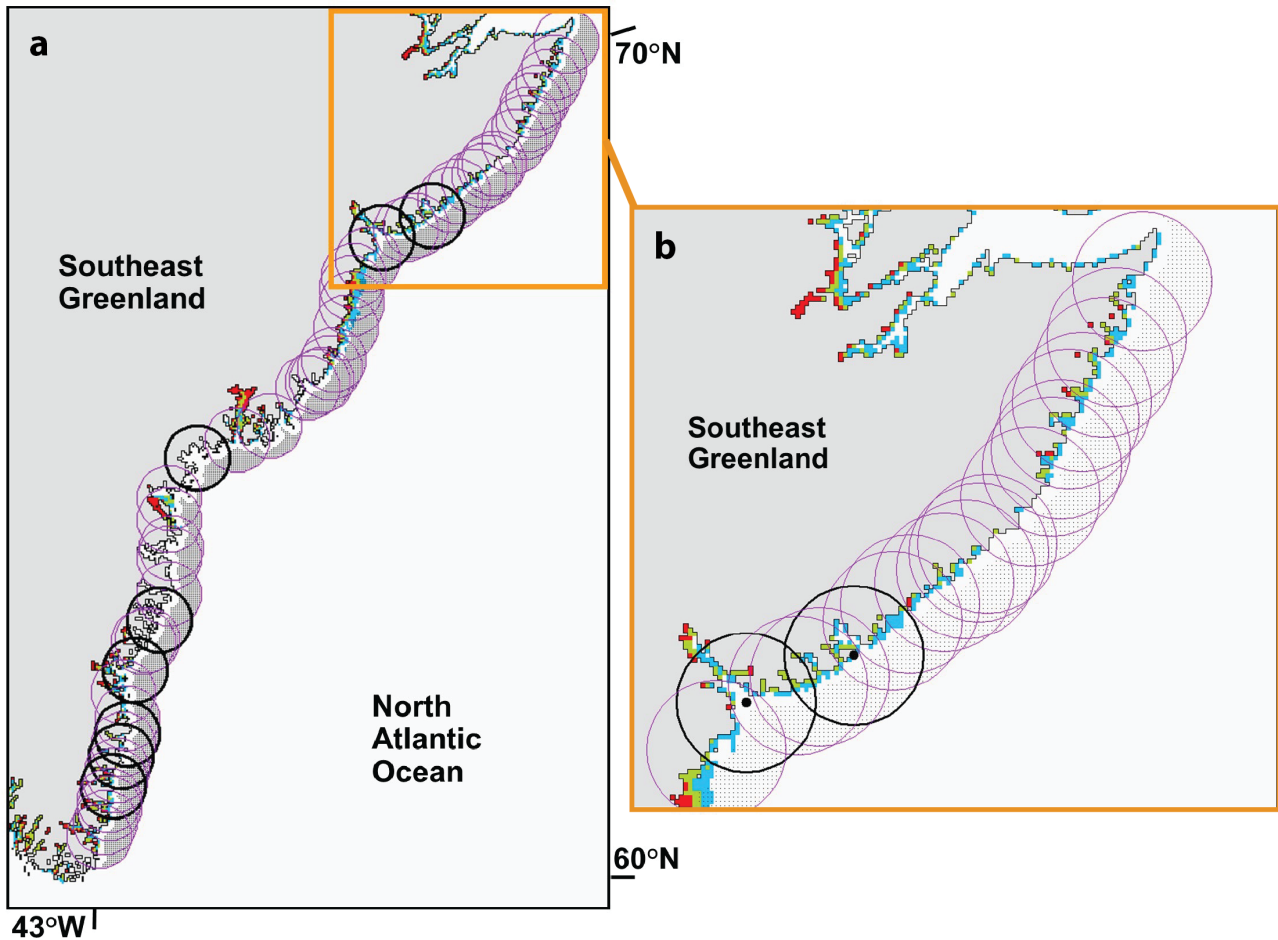
Figure 2. Regions at the mouths of (a) fjords 1-52 and (b) fjords 1-19 (circles of radius 50 km) for offshore sea-ice analysis. Small black dots indicate locations of gridded sea-ice concentration data from AMSR2. Grid cell size is approximately 3.125 × 3.125 km. A buffer zone of three grid cells from land is excluded from analysis due to land contamination of the ocean data, which can be seen in the form of spurious sea ice (red, green, and blue cells) for this date of October 2, 2013, when sea ice is almost surely not present along this portion of the coast. The black circles are associated with the focus fjords of this study.

3.3 Sea ice and sea surface temperature

To characterize the offshore sea ice at the mouths of the fjords, we used sea-ice concentration data derived from the passive microwave AMSR2 (Advanced Microwave Scanning Radiometer 2) instrument onboard the GCOM-W satellite operated by the Japan Aerospace Exploration Agency (Kaleschke and Tian-Kunze, 2016). The brightness temperature data were processed at the University of Hamburg using the ASI algorithm (Beitsch et al., 2014) to create daily gridded fields of sea-ice concentration with nominal grid cell size 3.125 × 3.125 km. We defined circles of radius 50 km centered at the mouths of the fjords (Fig. 2a). Within each circle we identified the offshore grid cells, excluding a buffer zone of three grid cells from land because the sea-ice signal in those cells may be contaminated by the signal from land (Fig. 2b). We then calculated the daily sea-ice area for the valid grid cells within each circle during 2015-2019. Figure 9a shows an example, in which the black curve is the daily sea-ice area, and the purple curve is a 31-day running mean. We defined a threshold equal to 15% of the mean March-April sea-ice area (horizontal black dotted line) and found the dates each year when the 31-day running mean crossed the threshold (vertical yellow dashed lines). The date in the spring when the sea-ice area drops below the threshold on its way to the summer minimum is called the spring transition date; the date in the fall when the sea-ice area climbs above the threshold on its way to the winter maximum is called the fall transition date. The transition dates for all fjords and all years are shown in Fig. 6.

To include further comparison metrics for sea ice coverage and also sea surface temperatures at the fjord mouth, we sampled output from MARv3.12 (Fettweis et al. 2017). MAR results have a grid resolution of 6.5 km, and we sample a single grid cell centered at the fjord mouth, which we extract based on fjord mouth outlines created as a subset of developing the SEG fjord boundaries (e.g., Fig. 1; Cohen et al., 2023). The MAR FRA variable identifies the open water and sea ice cover percentages, while the ST2 variable provides the sea surface temperature (SST) for open water and sea ice surface temperature. These are used together to determine the percent sea ice cover and the SST for the open water fraction. MAR has a hard-coded maximum sea ice cover of 95%, which we retain in our plotted results (e.g., Fig. 9e). Note that MAR assimilates SST and sea ice cover data from ERA5 available at a resolution of 0.3 x 0.3° (Hersbach et al. 2020).

3.4 Landfast sea ice for 8 focus fjords

To analyze landfast sea ice, we combined data extracted from imagery via the Operational Land Imager (OLI) onboard the USGS Landsat 8 satellite with data extracted from images captured by the Moderate Resolution Imaging Spectroradiometer (MODIS) instruments aboard the NASA Aqua and Terra satellites. There are notable differences between the two datasets: Landsat 8 imagery provides higher spatial resolution (30 m) with lower temporal resolution (16-day repeat cycle for each image footprint), while MODIS has lower spatial resolution (250 m) but higher temporal resolution (daily). Clouds and polar night limit the functional temporal resolution of both Landsat 8 and MODIS as the two satellites operate using optical sensors.

197 The suitability of every image from 1 January 2015 through 31 December 2019 in the region of interest was manually

198 inspected for use in our analysis. MODIS imagery was obtained from the NASA Worldview website

199 (https://worldview.earthdata.nasa.gov) and we downloaded the Corrected Reflectance (True Color) images that were

200 determined to be cloud-free (Fig. 3a). We used the USGS EarthExplorer web tool (https://earthexplorer.usgs.gov) to preview

201 all available Landsat 8 imagery and evaluate cloud cover (with a starting filter of 90% cloud cover). We downloaded cloud-

202 free Collection 1, Level 1 data (Fig. 3a) and we created multi-band natural color images using bands 4, 3, and 2. We used

203 both the R "stack" tool included in the "raster" package (https://cran.r-project.org/web/packages/raster/raster.pdf) and the

204 Composite Bands (Data Management) tool in ArcGIS to produce these composites. These composite imagery datasets were

205 catalogued and served as the foundation for further analysis.

206 Glacial ice, landfast ice, and pack ice share similar visual characteristics and are often adjacent to or intermixed with one

207 another within SEG fjords. Larger fjord systems, where active glaciers introduce glacial ice and large fjord mouths facilitate

208 the accretion of pack ice inside the fjords during the frozen season, are especially likely to contain a mixture of ice types.

209 This is compounded by the intricate geometry of these fjord systems, in which narrow corridors or tortuous coastlines entrap

210 ice of various types. Thus, we worked to distinguish landfast ice from glacier-derived ice, open water, and pack ice floes

211 (Fig. 4). By having one person complete the entirety of the visual digitization process, we attempted to reduce the potential

212 sensitivity of our manual analysis procedure.
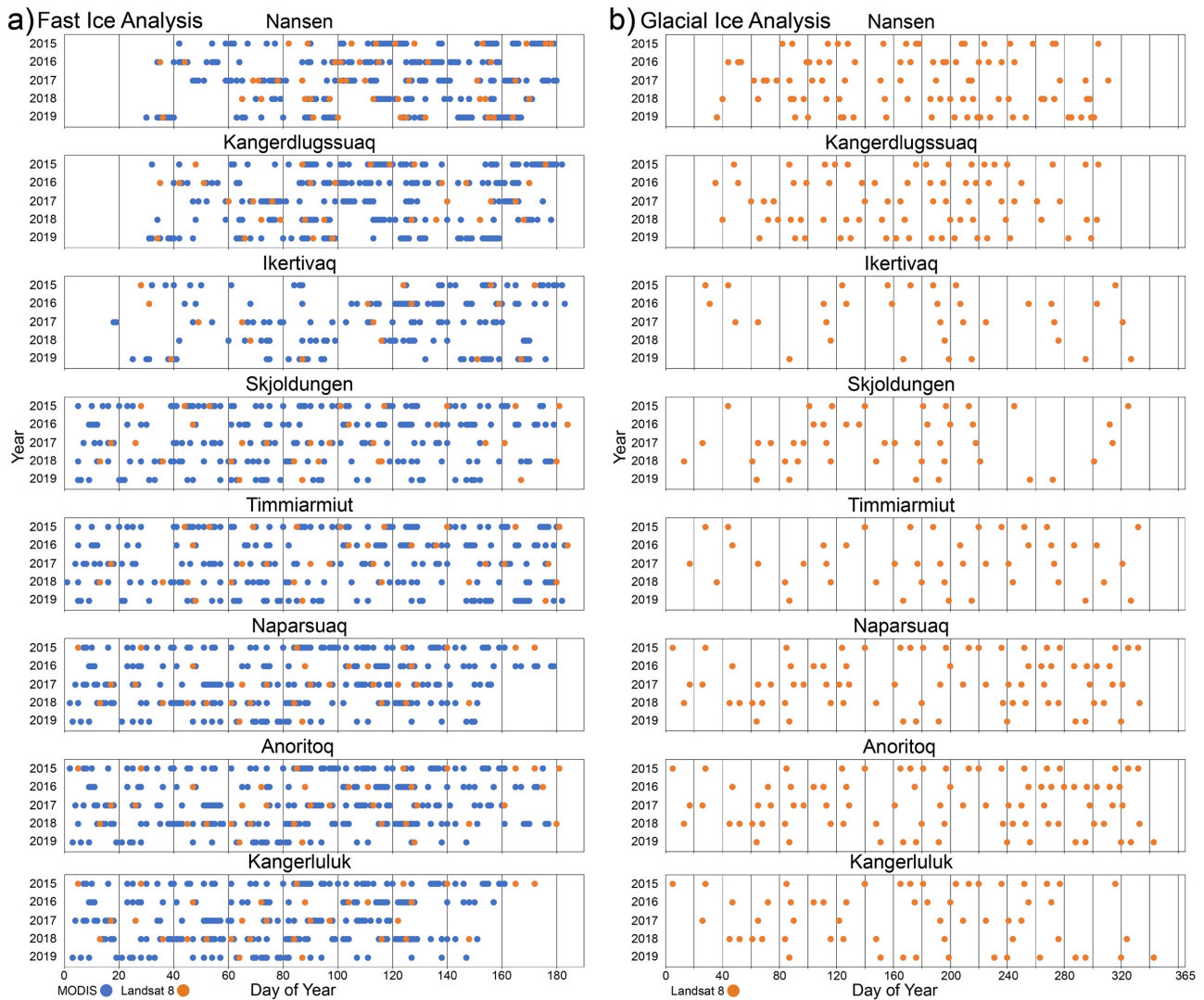
Figure 3. Availability of quality imagery data used for analysis during 2015-2019 for a) landfast ice analysis from MODIS and Landsat 8 images covering day 0-180 and b) glacial ice analysis from Landsat 8 images covering the full year.

213   Several visible characteristics in Landsat 8 imagery facilitated the identification of landfast ice: a smooth surface texture

214   (especially relative to glacier-derived ice); bright surface character; image-to-image persistence; and adhesion to coastal

215   boundaries. Landfast ice is more challenging to distinguish in lower-resolution MODIS imagery, where pixel color was the

216   most useful identifier along with image-to-image persistence. Several smaller regions in our study area were poorly resolved

217   by MODIS imagery, resulting in varying optical properties (e.g., color, saturation, brightness) for otherwise consistent ice

218   surface characteristics. To address this issue, the higher-resolution Landsat 8 imagery was analyzed first and produced

219   landfast-ice boundaries with a higher level of accuracy on the dates when such images were available. The MODIS imagery
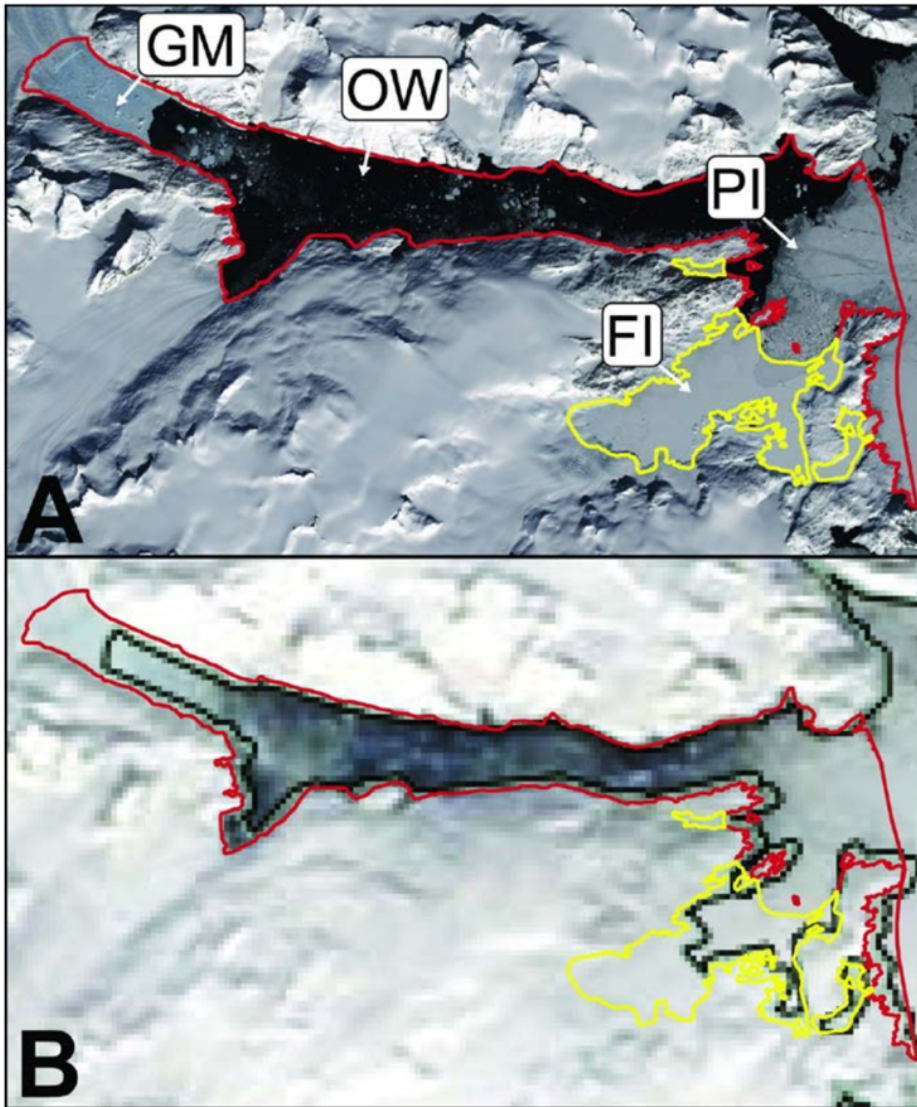
Figure 4. Example landfast ice digitization. (a) Landsat 8 and (b) MODIS image examples for Anoritoq fjord, both from 7 April 2017. Yellow outlines identify the fast ice areas and red lines indicate the rest of the fjord boundary. Note the distinct visual character of glacial mélange (GM), open water (OW), fast ice (FI), and pack ice (PI) (indicated in a). The misplacement of the coastline in the standard MODIS product is also apparent (b), and we use our own fjord boundary product for analysis. Figure reproduced from Laidre et al. (2022).

220   was processed afterwards, using the results of the Landsat 8 analysis as a guide for the characterization of MODIS imagery.

221   This facilitated increased accuracy of digitization within areas of ambiguous interpretation (as described below).

222   To quantify the degree of error introduced by using MODIS when Landsat 8 was unavailable, we digitized 25 MODIS

223   images (analyzing 1 image from 2015-2019 for Skjoldungen, Timmiarmiut, Naparsuaq, Anoritoq, and Kangerluluk fjords)

captured on the same date as Landsat 8 images already analyzed. We found a mean difference between the results of MODIS and Landsat 8 digitization of 1.2 km^2 of fast-ice area and a standard deviation of 12.6 km^2. These levels of disagreement have no significant impact on our conclusions.

Based on early results, landfast sea ice boundaries were analyzed starting on January 1 until either July 1 or ice-free conditions were reached (whichever was first) from 2015 through 2019. We digitized one Landsat 8 image from July 2, 2016 in fjords 37 and 40 as it showed end-of-season landfast ice melt conditions in high-resolution and allowed us to establish existence of ice-free conditions within 24 hours of our primary target time period. We manually delineated landfast-ice boundaries for each available image. Based on visual analysis, we traced landfast-ice boundaries (without regard to fjord edge boundary) and recorded the date and source of the image. Any portions of the resulting polygons outside of the fjord boundaries were erased using the Clip (Analysis) tool in ArcGIS, which resulted in fjord-surface measurements of landfast-ice area and percent area coverage. This method precluded repetitive and time-consuming fjord boundary tracing, allowing for more rapid digitization of landfast ice.

After calculating the landfast-ice area in a fjord system from all available imagery within a single year, we applied a moving average to obtain a smooth representation of the formation and breakup of landfast ice. The moving average on day t is calculated using weights proportional to $\exp(-\Delta t^2/T^2)$ where Δt is the number of days from t to other data points, and T is a time scale equal to 7 days. To demonstrate the likelihood of landfast ice presence in any given spatial region across all observations, we also produced "heatmaps" of landfast sea ice presence (Figs. 10-13a,c) by overlaying all individual spatial occurrence maps and applying a gradient of shading (applying grid cell size of 50 m x 50 m).

3.5 Glacier-derived ice for 8 focus fjords

To analyze glacier-derived ice, we again used USGS Landsat 8 data imagery (following section 3.4 methods). The low spatial resolution of MODIS imagery made it unsuitable for this analysis. Because glacial ice has a year-round presence, we analyzed glacial ice presence from 1 January to 31 December for each year (Fig. 3b).

We characterized glacier-derived ice using four primary categories (Fig. 5, Table 2): spatially dense glacial ice mélange (type 3); moderately high-spatial-density, mixed-size glacier-derived ice with large icebergs (type 2); low-spatial-density glacier-derived ice with large icebergs (type 1); and consistent small-ice surface without large icebergs (type 0). (We also used a 'type 99' classification for glacier ice not yet calved). To measure the temporal and spatial distribution of glacier-derived ice in SEG, we analyzed the optical satellite imagery from Landsat 8 using the same ArcGIS 10.8 method as described for landfast sea ice for each glacier-derived ice type (Table 2). For the heatmaps of glacial ice presence (Figs. 10-13b,d), we combine spatial extent for type 2 and type 3 glacier-derived ice. This is motivated by an assessment that type 2 and type 3 glacier-derived surface ice is more feasible for use as polar bear habitat platforms (e.g., Laidre et al., 2022).
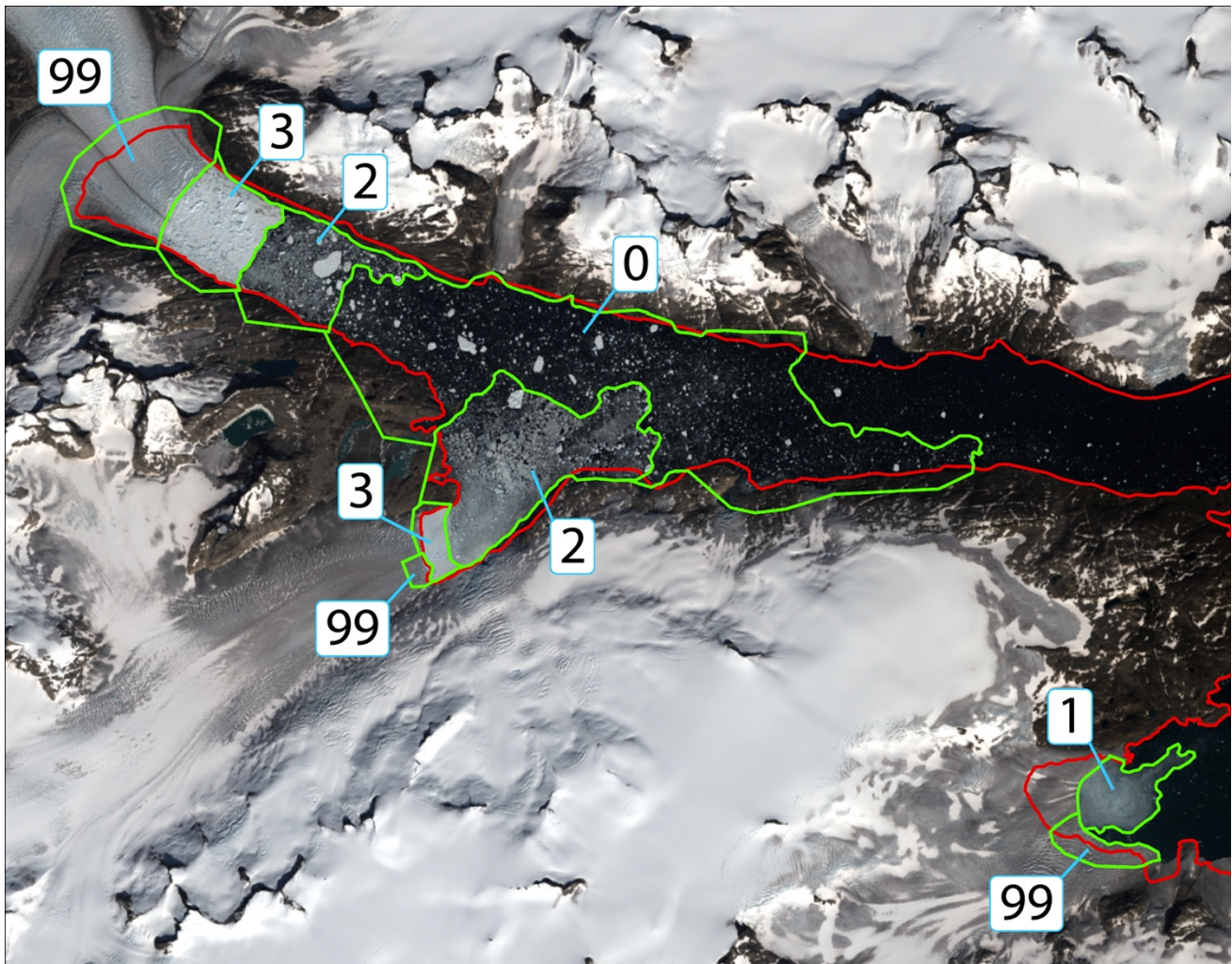
Figure 5. Example glacial ice digitization for Anoritoq fjord (fjord 45). Landsat 8 background image (8/1/15) showing the fjord boundary (red outline) and the digitized zones of different glacier-derived ice types on the fjord surface (green outlines with type indicated): type 3 (dense glacial mélange), type 2 (mixed glacier-derived ice), type 1 (small glacier-derived ice), type 0 (highly dispersed glacier-derived ice), and type 99 (glacier surface) (see Table 2). The boundaries are combined to determine final values for glacier-derived ice area.

4 Results

This study includes data sets that span Southeast Greenland and metrics assessed only for the eight focus fjords. This supports some SEG region-wide analysis and further analysis to include more ocean-surface ice metrics for the eight focus fjords. Along with providing a more complete picture of the SEG environment, these results can support ongoing research into the current and future biological uses of SEG coastal fjords.

Table 2: Glacier-derived fjord ice types as applied in this analysis.

Glacial ice type	Description used for manual digitizing
Type 3 (dense glacial mélange)	White to pale to blue color. Color (considering variation in texture) consistent throughout with bright, vibrant character Appears potentially cohesive, without open water gaps. May have sharp edge boundaries Texture: clear inclusions of many icebergs Also digitize very large (~>1km width) mélange platforms
Type 2 (mixed glacier-derived ice)	Majority of ice colored grayish blue of varying shades with semi-transparent character Discernible floes of apparently glacial origin, varying size with inconsistent cohesion and potential presence of small (~<250 m) open water gaps. Possible presence of Type 3 platforms Includes sizable icebergs
Type 1 (small glacier-derived ice)	Gray blue to dark blue coloration with higher degree of transparency compared to Type 2 and Type 3 ice Little to no cohesion, but still high spatial concentration of likely growlers/bergy bits. Few icebergs and Type 3 platforms of any substantial size, but not absent
Type 0 (highly dispersed glacier-derived ice)	Concentration of icebergs of moderate size (~250 m width) > 10% and <30% Little slushy (grey) background ice (bergy bits, growlers)
Type 99 (glacier surface)	Glacier surface. Sections of glacier ice not yet calved but inside the fjord boundary.

4.1 Regional-scale observations

Datasets for offshore sea ice, freshwater flux, and solid ice discharge support an examination of conditions across the full SEG region of interest.

4.1.1 Offshore sea ice

Figure 6 shows the spring and fall transition dates for offshore sea ice at each fjord. First, while there is substantial year-to-year variability in the spring transition dates, which range from May to early August, there is little variability with latitude for a given year. In other words, offshore sea ice tends to disappear from the coast of SE Greenland in spring over a relatively short time interval across all latitudes, but the timing of that disappearance varies from year to year. Second, the arrival of offshore sea ice in the fall has a narrower range of interannual variability, but there is a distinct dependence on latitude, with sea ice arriving in October at the more northerly fjords and in January or early February at the more southerly fjords. The different nature of the spring and fall transition dates may be due to the relative influence of thermodynamics vs. dynamics. In spring, rising temperatures along the coast may melt the sea ice at more-or-less the same time at all latitudes. But in fall, the arrival of sea ice is due to transport from the north (via the East Greenland Coastal Current) rather than freezing in place. A sea-ice "front" progresses from north to south every fall, at a speed of roughly 10 km day^{-1} (Fig. 6). Note that previous research identified that sea ice along the SEG coast had a mean wintertime (January-April) south-moving speed
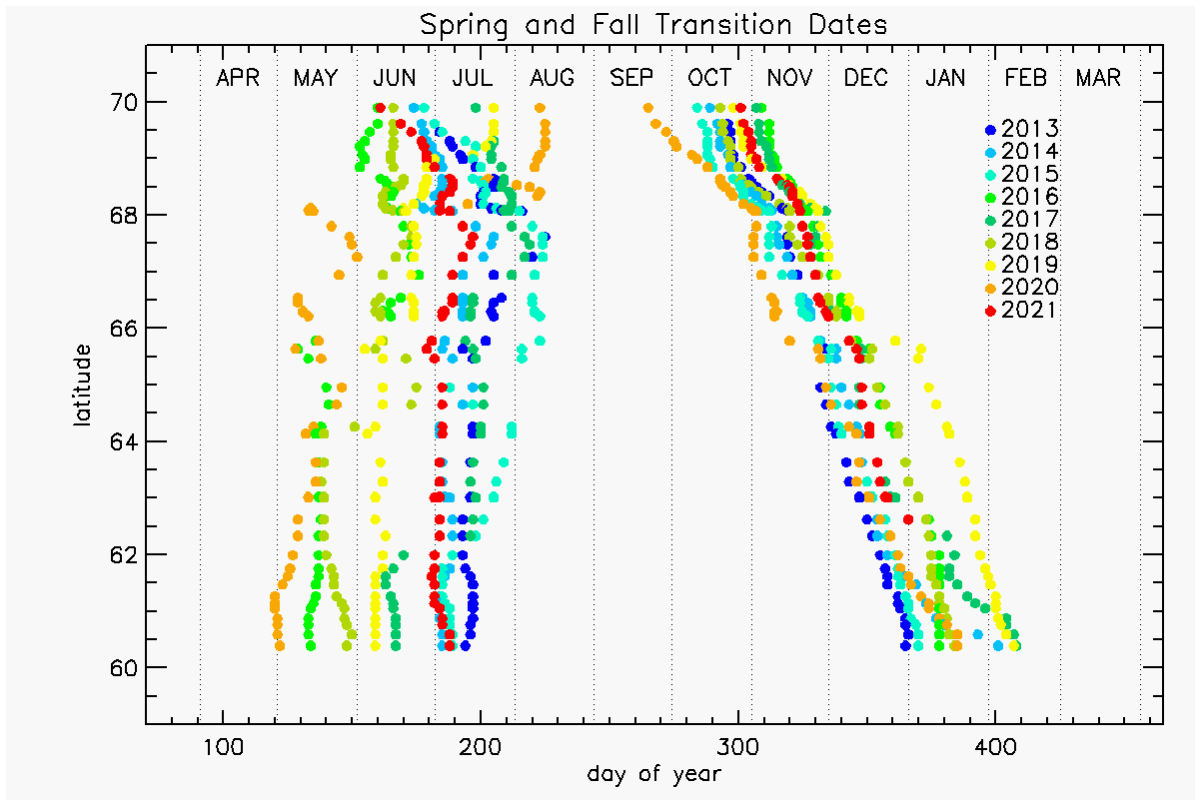
Figure 6. Spring and fall transition dates of offshore sea ice for all fjords (by latitude) and years (by color) based on a 15% coverage threshold.

274 of about 15 cm s^{-1} (13 km day^{-1}) from 2010 to 2018 (Laidre et al., 2022). In spring, the sea ice does not retreat along a well-

275 defined front. Though the seasonal coverage and concentration of offshore sea ice during our study period is reduced from

276 earlier decades (Heide-Jørgensen et al. 2022) and is expected to continue to shorten and decline, respectively (Kim et al.,

277 2023), we suggest that the differences in spring and fall transitions may largely persist (while sea ice is still forming).

278 **4.1.2 Freshwater flux**

279 Figure 7 shows freshwater flux on the fjord scale across SEG. The results show that there is large variability, from low total

280 annual discharge of ~1x10^8 m^3 (~0.1 Gt) at fjords 6 and 44 up to ~1.25x10^{10} m^3 (~12.5 Gt) at Sermilik Fjord (fjord 30),

281 though notably the next largest fjord freshwater fluxes are only 8.48x10^9 m^3 (8.48 Gt; Kangerdlugssuaq, fjord 18) and

282 7.12x10^9 m^3 (7.12 Gt; Jens Munk, fjord 33). In the northern region of SEG, the catchment geography feeds much of the

283 freshwater to fjord 5, while other fjords in that zone see little freshwater flux until reaching south to fjord 15 and then to

284 fjord 18 (Kangerdlugssuaq). There's low to moderate flux for most fjords between 18 and 30 (Sermilik), with a notable

285 increase in mean annual freshwater flux for a number of fjords south of Sermilik.
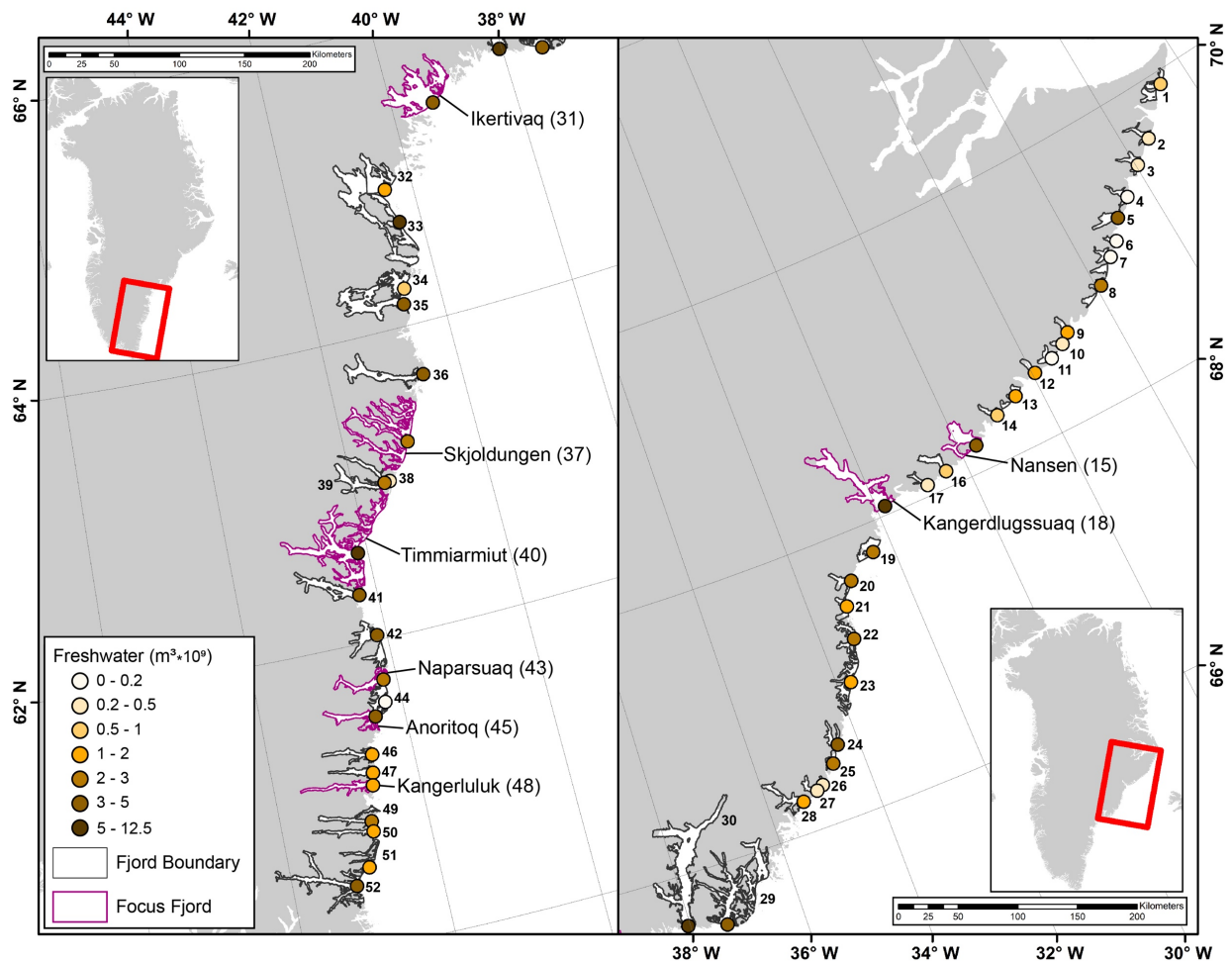
Figure 7. Mean total annual freshwater flux (m³x10⁹) for 2015 through 2019. The freshwater discharge is summed for the full fjord, including melt that originated from ice-covered and terrestrial areas and sourced from Mankoff (2020) and Mankoff et al. (2020a). Note that for freshwater, 1 m³x10⁹ volume is equivalent to 1 Gt weight.

286   Using the discharge elevation/depth, we were also able to assess how much freshwater was entering fjords at the ocean

287   surface or at depth, discharging from under marine-terminating glaciers. Across the SEG study region, the ocean surface

288   input and 0-20 m depth bins receive the most input when considering flux through sea level to 1000 m depth (Fig. A2).

289   Across the region and looking deeper into the water column, flux totals are highest within the top 100 m. While flux is

290   measured as deep as 900 m (fjord 31, Ikertivaq), most flux occurs at depths shallower than 600m. Strong seasonal variability

291   in freshwater flux is also apparent (e.g., Fig. 9c). Detailed individual fjord plots are available via our research code (see Code

292   and data availability).

4.1.3 Solid ice discharge
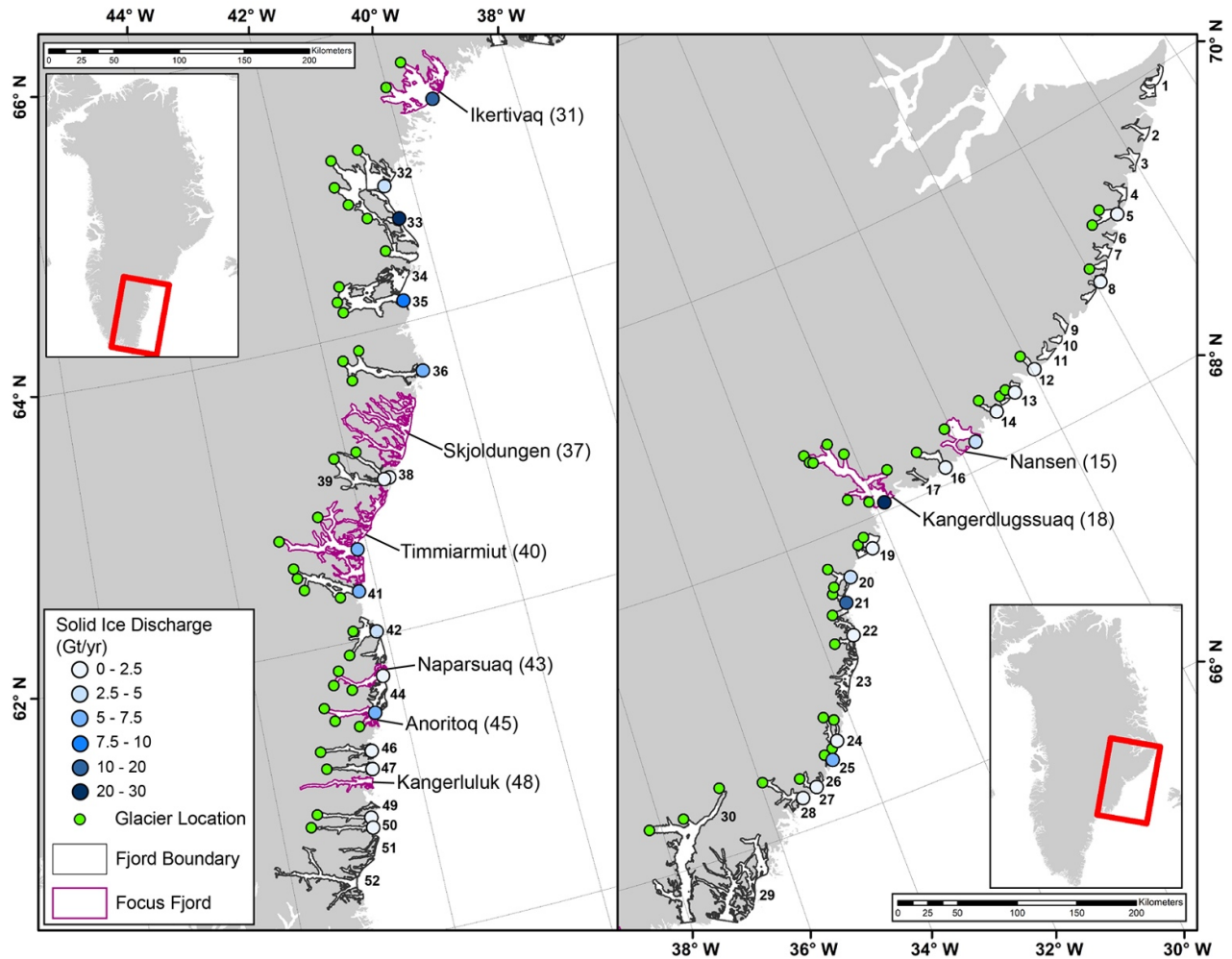
Figure 8. Mean annual solid ice discharge (Gt yr⁻¹) during 2015 through 2019 for glacier-derived ice from indicated glaciers, calculated using Mankoff et al. (2020b).

Figure 8 shows annual solid ice discharge estimates. We used a fjord-scale perspective to examine solid ice discharge and relied on the availability of glacier solid ice discharge data from Mankoff et al. (2020b, 2020c). Because of this, our solid ice discharge values may underestimate discharge or provide no data for a fjord in which some glacier-derived ice is variably present. For example, the source dataset contains no glacier discharge data for Skjoldungen fjord even though glacier-ice inputs are apparent in our satellite image analysis (Figs. A5 and 11d). Within the fjord dataset we were able to create (Fig. 8), fjords north of Sermilik have relatively small annual contributions of glacier-derived ice, with the exception of Kangerdlugssuaq (fjord 18) and, to a lesser extent, fjord 21. Slow flow rates and often relatively thin glacier termini in this region are the cause of the low glacier-derived concentrations in many fjords, especially for the Geikie Plateau, where most
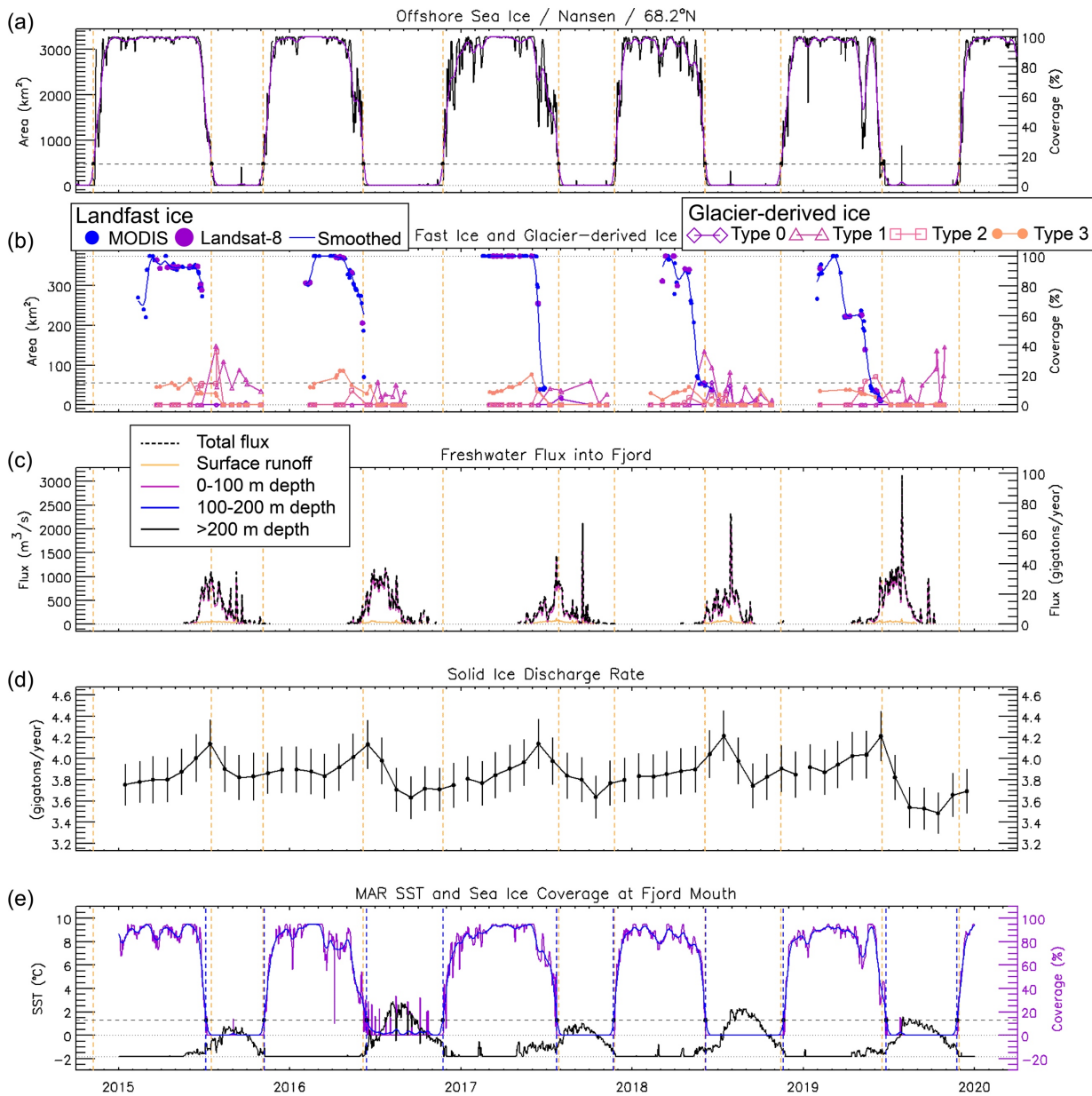
Figure 9: Time series for fjord 15 (Nansen) showing: a) daily (black line) sea-ice area (km²) and percent coverage based on AMSR2 sea ice concentration, along with a 31-day running mean (purple), b) area (km²) and percent coverage for landfast ice evaluated from MODIS (blue dot) and Landsat 8 (purple dot) single image sources and with smoothed (blue) record and for all four surface character types (0-3) for glacier-derived ice, c) total freshwater flux (m³ s⁻¹, black dashed line) and depth-binned (solid line) freshwater flux, d) cumulative fjord solid ice discharge (Gt yr⁻¹), and e) sea surface temperature (black line) and sea ice coverage (purple line) measured at the fjord mouth from MAR climate data. Vertical dashed orange lines in all panels indicate the freeze-up and break-up dates for offshore sea ice (panel a) as measured by passing a threshold of 15% of mean March-April sea ice area. A similar threshold is indicated (dashed line) in panel e, while panel b is a simple 15% threshold (dashed line). Similar figures are provided in Appendix A for other focus fjords.

302   glaciers may be considered part of a peripheral ice cap (Rastner et al., 2012). By contrast, Ikertivaq and a number of fjords

303 south of Sermilik are fed by several glaciers, many of which receive moderate and greater levels of solid ice discharge.

304 **4.2 Focus fjord observations**

305 Manual analysis of landfast sea ice and glacier-derived ice allows us to integrate these observations and compare across

306 metrics. Figs. 9 and A3-9 provide stacked 2015-2019 time series of offshore sea ice area and percent coverage; landfast ice

307 and glacier-derived ice area and percent coverage; freshwater flux binned into sea surface input and input at depths of 0-100

308 m, 100-200 m, and >200 m; cumulative fjord solid ice discharge; and fjord mouth SST and sea ice coverage from

309 MARv3.12. These give a sense of temporal evolution across a range of latitudes. In contrast, Figs. 10-13 home in on results
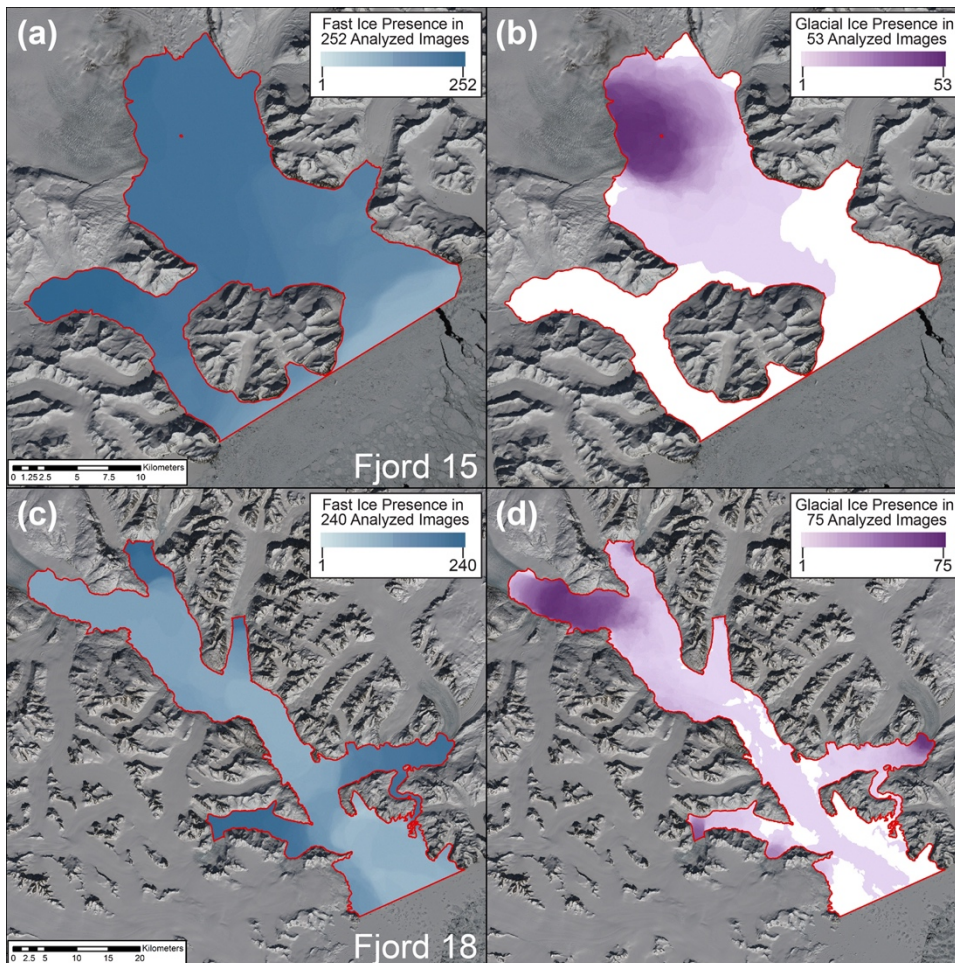
Figure 10. Maps of fast ice presence (a and c) and glacial ice presence for types 2 and 3 (b and d) for fjord 15 (Nansen, top panels) and fjord 18 (Kangerdlugssuaq, bottom panels). Map symbology is relative to the number of images analyzed (noted in panel legends).

310 of the landfast and glacier-derived ice analysis to provide a spatial map-view for the presence of landfast ice and types 2 and
311 3 glacier-derived ice.

312 Across all eight focus fjords, landfast ice regularly accumulates in particularly narrow fjord "corridors" (narrow areas of the
313 fjord with entrances/exits for ice flux on either end; e.g., Fig. 11a, c) and/or the "corners" of fjords (areas with a single
314 entrance/exit for ice flux and a confined coastal topography; e.g., Fig. 12a, c). The Nansen (fjord 15) and Kangerdlugssuaq
315 (fjord 18) fjords display periods in which they are fully covered by landfast ice in certain years, while all the more southerly
316 fjords do not reach full landfast ice coverage in any study years.

317 Despite broad seasonality and spatial consistency to landfast ice development, there is substantial year-to-year variability for
318 landfast ice development within each fjord (panel b within Figs. 9 and A3-9). When considering a 15% landfast ice coverage
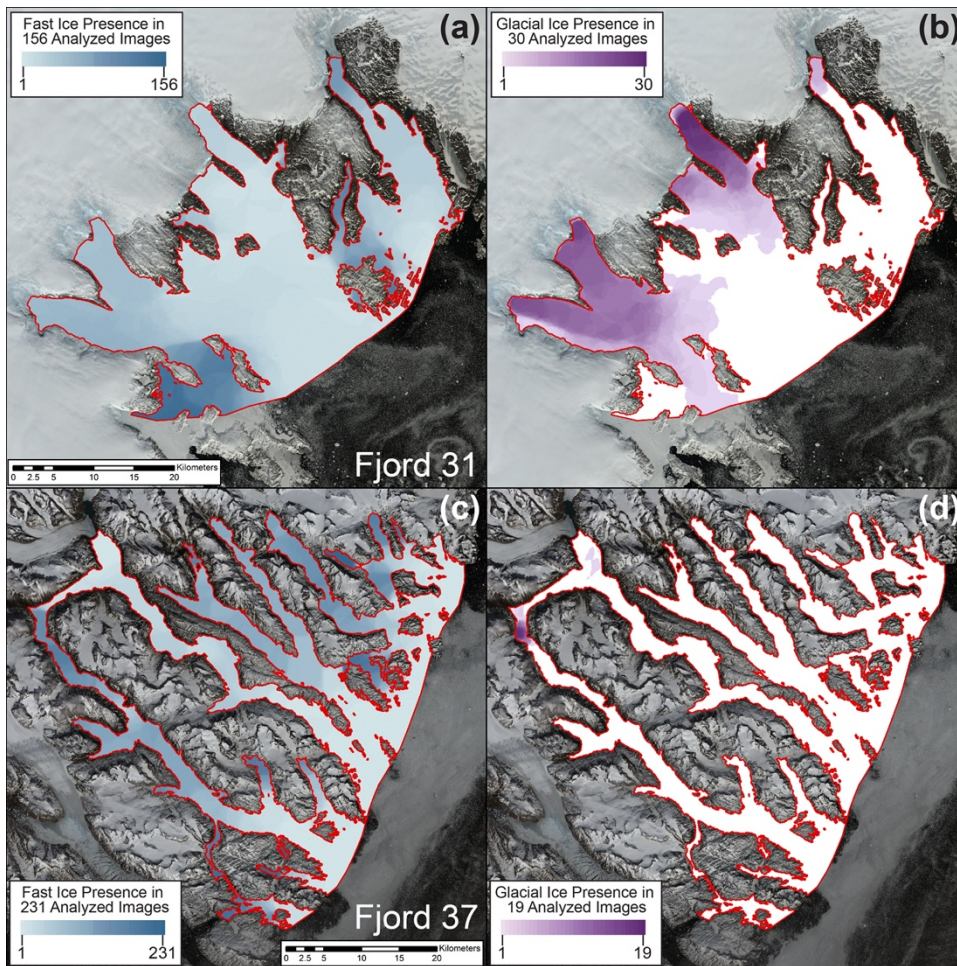
Figure 11. Same as figure 10 for fjord 31 (Ikertivaq, top panels) and fjord 37 (Skjoldungen, bottom panels).

threshold, more northern five focus fjords have lower variability in the timing of landfast ice development and breakup, but the timing of the fast-ice peaks has substantial variability (Table A1). For example, in 2017 in Ikertivaq the landfast ice was slower to form, with some expansion/decline, before peaking at close to 80% area coverage in late April, while in 2019 Ikertivaq experienced a relatively rapid development of landfast ice with a similar area coverage peak in early March (Fig. A4). For the three southernmost fjords there is larger variability in the timing of the formation and breakup of the landfast ice. Landfast ice did not surpass a 15% ice coverage threshold for Naparsuaq in 2019, Anoritoq in 2015, and Kangerluluk in both 2015 and 2019 (Figs. A7-9). Yet, we do observe clear instances of landfast ice remaining in place well-after offshore sea ice has fully disappeared, with many of the focus fjord declines in landfast sea ice lagging the offshore sea-ice declines by more than a month in 2016 and ~two weeks in 2018 (panel b within Figs. 9, A3-9).

Glacier-derived ice presence for types 2 and 3 combined (Figs. 10-13b,d) is dependent on marine-terminating glacier locations, with higher presence near the glacier termini. As expected, the manually digitized imagery also highlights glacier
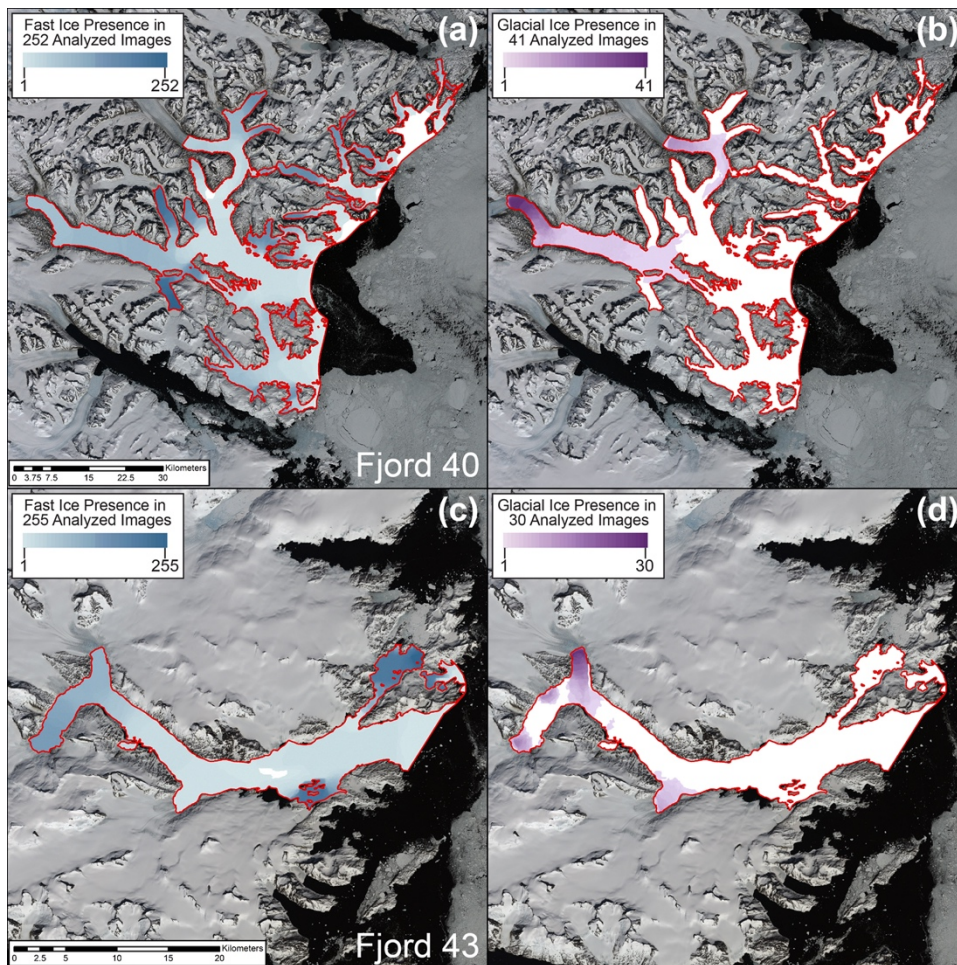
Figure 12. Same as figure 10 for fjord 40 (Timmiarmiut, top panels) and fjord 43 (Naparsuaq, bottom panels).

ice inputs that may be absent in other datasets (such as we use for regional SEG solid ice discharge). Because of landfast ice and glacier-derived ice intermixing (or at minimum an inability to distinguish boundaries from satellite imagery), our results highlight glacier-derived ice-dominant or landfast ice-dominant fjord regions rather than consistent or clear delineations within most fjord regions. The time series of glacier-derived ice (Figs. 9, A3-9) indicate that only Kangerdlugssuaq, Ikertivaq, and Anoritoq more regularly contain types 2 and 3 glacier-derived ice outside of that fjord's landfast ice season.

Finally, we compared the spring and fall sea ice transition dates as calculated from AMSR2 sea-ice coverage (e.g. Fig 9a, vertical dashed orange lines, repeated in all panels) vs. MAR sea-ice coverage (e.g. Fig 9e, vertical dashed blue lines) for the eight focus fjords. For the three northern fjords (fjords 15, 18, 31), which are all north of 64N, the agreement is quite good: the mean dates (across 5 years) are within 3 days of each other. These fjords have relatively well-defined annual cycles of sea-ice coverage, so there is little ambiguity in identifying the transition dates. For the five southern fjords, which are all south of 64N, the agreement is less good: mean differences can be as high as +/-16 days, with larger variability than for the northern fjords. These fjords have relatively large swings in the wintertime sea-ice coverage, including lots of spikes, so the detection of the transition dates is noisier. For the four most southerly fjords (fjords 40, 43, 45, 48), there are instances of MAR dates both earlier and later than AMSR2 dates for spring and fall transitions. In contrast, the MAR-based threshold is consistently earlier (or the same) for the spring transition and later for the fall transition at Skjoldungen (fjord 37). For cases with high sea-ice coverage variability, we suggest using other metrics (e.g., mean wintertime sea-ice coverage) for comparing MAR vs. AMSR2 accuracy and agreement.
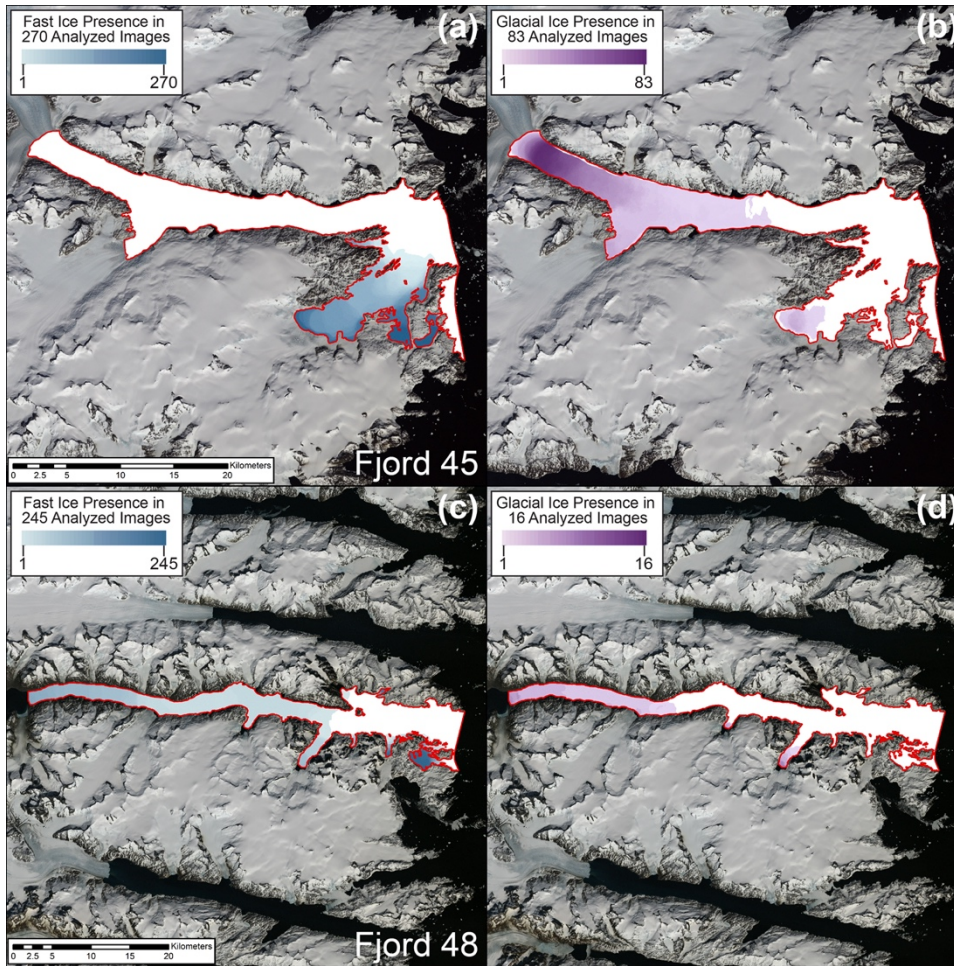
Figure 13. Same as figure 10 for fjord 45 (Anortioq, top panels) and fjord 48 (Kangerluluk, bottom panels).

4 Discussion

Factors affecting ice in SEG fjords can be broadly divided into two categories: (1) relatively fixed factors such as fjord width, length, bathymetry, orientation, latitude, and locations of glaciers feeding into the fjord; and (2) variable factors such as katabatic winds coming off the ice sheet, along-shore winds driven by cyclones, ocean currents, ocean stratification, ocean heat content, air temperature, formation of sea ice, and the discharge of freshwater and glacial ice into the fjord. The formation of landfast ice and accumulation of glacier-derived ice in SEG fjords tends to have a semi-consistent spatial pattern; landfast ice and glacial ice can be found in similar areas within each individual fjord from year to year (Figs. 10-13). This distribution is likely a combination of fixed and variable factors. For example, the morphology of each fjord system is likely a first order control. Variable factors such as ocean currents may also produce relatively consistent ice conditions, but

current and future potential for ocean variations have to be considered. For example, as the East Greenland Coastal Current flows past the mouth of a fjord, it turns to the right (due to Coriolis) and enters the fjord, keeping the shoreline on the right. The current flows into the fjord along the north or east side of the fjord, then out along the south or west side of the fjord, influencing ice-forming surface conditions and iceberg motion in the process. But the flow is not steady in time. Recent examination of four East Greenland fjords, including two in SEG (Kangerdlugssuaq and Sermilik), found periodicity in current patterns in the range of 2-4 days for Kangerdlugssuaq, plus a broad peak around 10 days (Gelderloos et al., 2022). Thus, factors still not included in this study warrant examination and future synthesis.

Temporally, landfast ice and glacial ice follow different patterns. Landfast ice forms seasonally from roughly February to late May, with significant inter-annual variability of cover duration (Table A1), while glacier-derived ice can be found in various fjords year-round. However, the character (e.g., type 0-3), timing, and area coverage of glacier-derived ice is strongly fjord-dependent, with even some glacier-fed fjords appearing to provide little possibility for substantial glacier-derived ice habitat outside of the landfast ice season.

Of note regarding our mapping of landfast ice locations is that they commonly appear in areas that remain poorly mapped for bathymetry. Comparing landfast ice locations with bathymetric data from BedMachine 5 (Morlighem et al., 2017; Morlighem et al., 2022), for example, landfast ice often occurs in presumably shallow regions that lack any bathymetric detail. Greenland sea level responses to climate change include the possibility for local regions to experience falling sea levels (Fox-Kemper et al., 2021). This suggests that understanding shallow-region bathymetry will only become more important, though the sea level changes may occur much slower than some other global coasts. For example, changes in ocean depth have the potential to influence wave character, which contributes to mechanical landfast ice breakup (Petrich et al. 2012), and the prevalence of possible grounding points, which may influence landfast ice formation (Mahoney et al. 2014). These shallow regions, which we speculate are mostly ~0-50 m depth, may also experience substantially different heat budget processes, as they are shallower than potential warm Atlantic water inflows and may also be less involved in largescale fjord water circulation systems.

Glacier-derived ice, produced from marine-terminating glaciers in SEG fjords, is initially deposited at the glacier terminus and proceeds to drift into the fjord as it melts, fractures, and disperses. As glacial ice travels through the fjord system, it can become trapped amongst forming landfast ice and thus effectively adding to the landfast ice itself. This is especially frequent in narrow, long fjords where landfast ice can clog passageways and prevent glacial ice from exiting the fjord at the mouth. This heterogeneous mixture of frozen landfast ice and glacial ice provides stable optimal springtime habitat for ice-breeding seals, as well as foraging polar bears (Laidre et al., 2022). The distribution of glaciers across SEG (e.g., Fig. 1) is heterogeneous, with some fjord systems having multiple productive glaciers (e.g., fjords 18 and 31) while others have minor or no glacier-derived flux (e.g., fjord 37). It is unclear from our observations the extent to which glacier-derived ice either enhances landfast ice persistence or diminishes it. For example, production of glacial ice in fjord 15 may help to compress and possibly thicken landfast ice (Fig. 10a,b), especially if paired with sea ice circulating into the fjord from offshore. On the

other hand, glacial ice traversing from a glacier terminus towards the fjord mouth might shear against the landfast ice edges, particularly if they are subject to different wind or current forces, for example due to different surface heights and bottom-ice depths.

Differences in offshore sea ice and landfast ice development across SEG suggest that glacier-derived ice may be especially important as a fjord surface ice environment, though there is substantial interannual variability (Figs. 9a, b, e, A3-9a, b, e). Earlier research demonstrated that the 1999-2018 mean width of the offshore wintertime sea-ice band for 60-65°N was 19 km, while for 65-70°N it was 149 km (Laidre et al. 2022). The four most southerly focus fjords functionally experienced no full coverage of offshore sea ice throughout 2015-2019 (Figs. 9a, A3-9a). Combined with low landfast ice coverage, animals may have limited options for sea ice platforms, while glacier-derived ice is present to some extent in all of these fjords. The extent to which limited and sporadic coverage of glacier-derived ice (Figs. 9b and A3-9b) provides year-round ice habitat is unknown, but observations and tracking data of top predators suggests animals use this habitat year-round for hauling out (e.g., resting) or foraging (Laidre et al., 2022).

5 Conclusion

Fjords across Southeast Greenland exhibit high fjord-to-fjord variability in regards to bathymetry, size, shape, and glacial setting. As a result, some fjords receive substantially higher annual freshwater flux from ice sheet/glacier and terrestrial runoff, as well as fjords with much higher presence of glacier-derived ice. The inputs mix with in-fjord sea ice and landfast ice and offshore sea ice to create a dynamic fjord surface environment.

Across 2015 through 2019, SEG fjords demonstrate substantial year-to-year variability. While the impacts of climate change may be expected to push long-term trends in one general direction, the variability in separate metrics will likely be different. For example, the sensitivity of freshwater flux to ice sheet surface melt introduces a high dependency on atmospheric conditions, which change rapidly and have high inter-annual variability (Lenaerts et al., 2019). On the other hand, solid ice discharge depends on ice sheet and glacier dynamics, which generally respond more slowly to climate change and have lower inter-annual variability (Moon et al., 2022), and ocean conditions. Landfast sea ice variability introduces further dependence on ocean surface conditions, which are also a major factor for formation of mobile sea ice.

With ongoing sea-ice loss along the east coast of Greenland (Stern and Laidre, 2016) and projections for summer sea-ice free conditions to occur within one to two decades (Kim et al. 2023), the importance of glacier-derived ice as a habitat for top predators may only rise. Projections for the spatial patterns of Greenland Ice Sheet retreat under a range of future scenarios point towards the longer-term presence of glacier ice in SEG compared to other coastal areas (Aschwanden et al., 2019; Bochow et al., 2023). High winter precipitation in SEG as compared to other regions (Gallagher et al., 2021) is one important factor in sustaining glacier ice in the region. This higher regional winter snowfall may also provide longer-term habitat appropriate for ringed seal birthing lairs, which are created as on-sea-ice snow caves with sufficient snow cover

420 associated with lower predation rates (Kelly et al., 2010). Further, the heterogeneous mix of glacial ice frozen into the fast

421 ice can provide suitable drifts for ice seal birth lairs, which can form quickly on any side of an iceberg given their complex

422 geometry. This has also been seen in the case of polar bear maternity dens in Northeast Greenland (Laidre and Stirling

423 2020). As a result, there is a potential for SEG to remain a long-term (century to millennia scale, dependent on future climate

424 change pathway) refugia location for polar bears and other ice-dependent wildlife, but further investigation is required to

425 quantitively assess this potential.

426 **Appendix A**
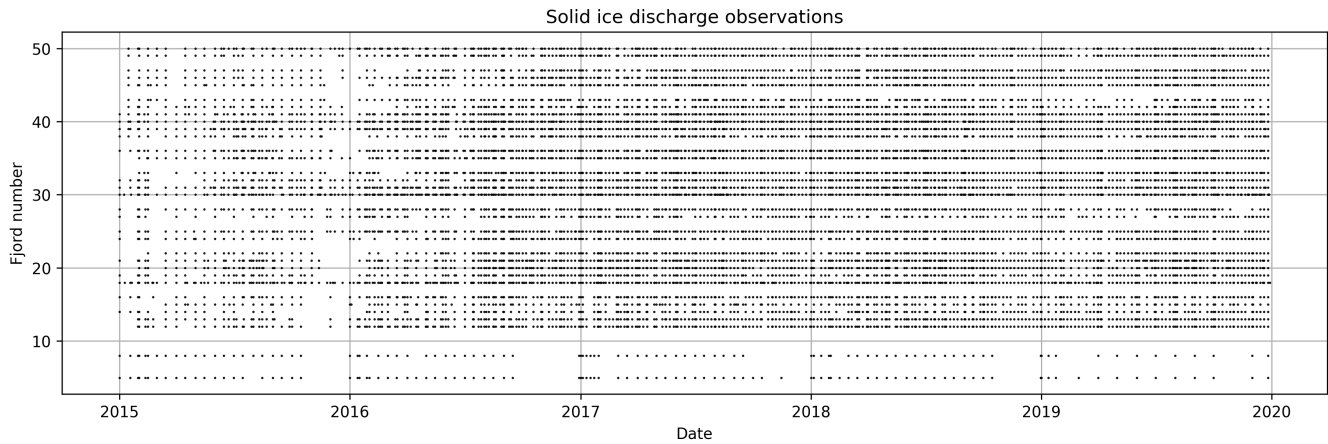
427
428 **Figure A1. Distribution of solid ice discharge observations during 2015 through 2019 for all Southeast Greenland fjords based on**
429 **fjord number (see Fig. 1).**
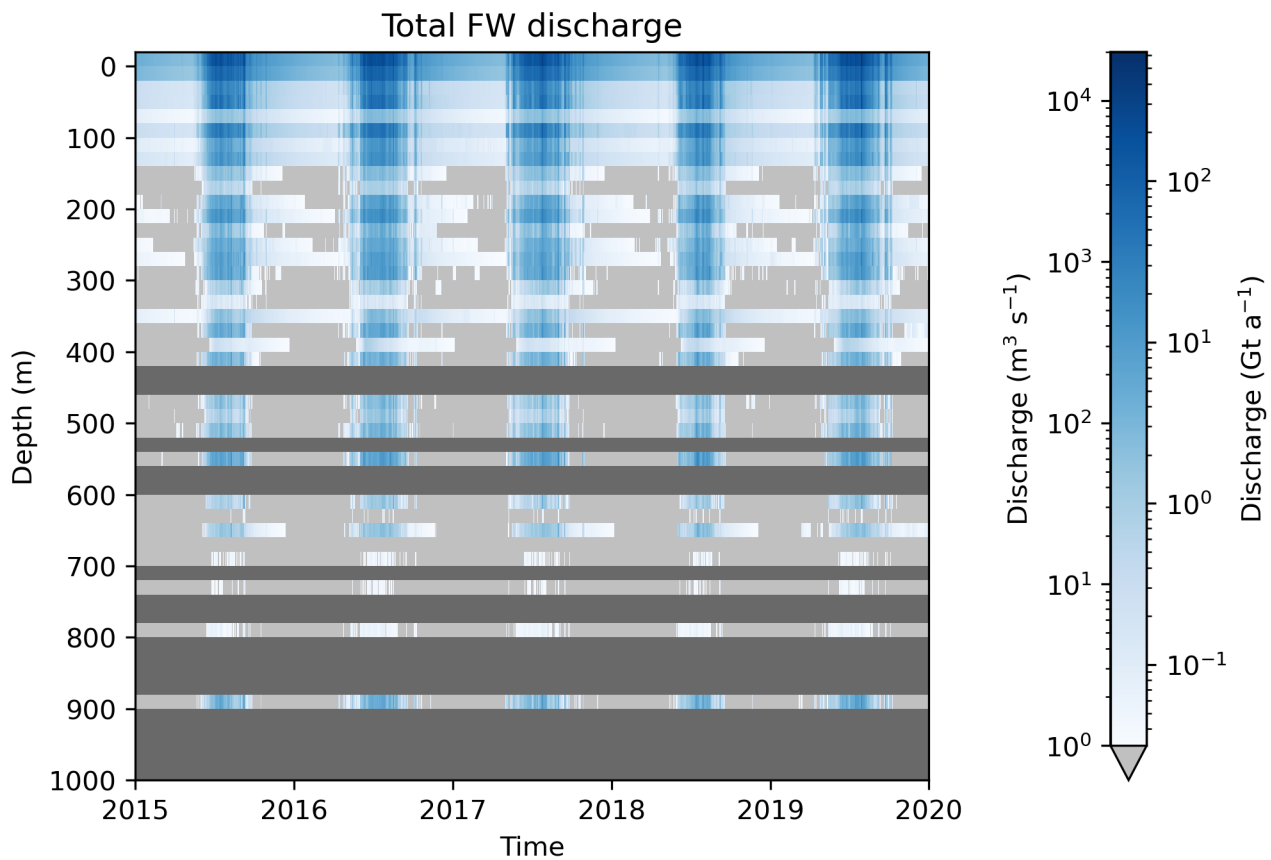
430

431 **Figure A2. Total freshwater (FW) discharge within SEG fjords during 2015 through 2019, representing only data within Mankoff**

432 **(2020) and Mankoff et al. (2020a). Freshwater discharge is binned into 20-m segments, from +20 – 0 m asl (above sea level) to 980 –**

433 **1000 m depth, with all discharge from elevations above 0 m asl included in the +20 – 0 m asl bin. Light gray areas indicate times**

434 **when the discharge in that bin was below a discharge threshold of 1 m^3 s^{-1}, while dark gray areas indicate depths without subglacial**

435 **discharge outlets.**
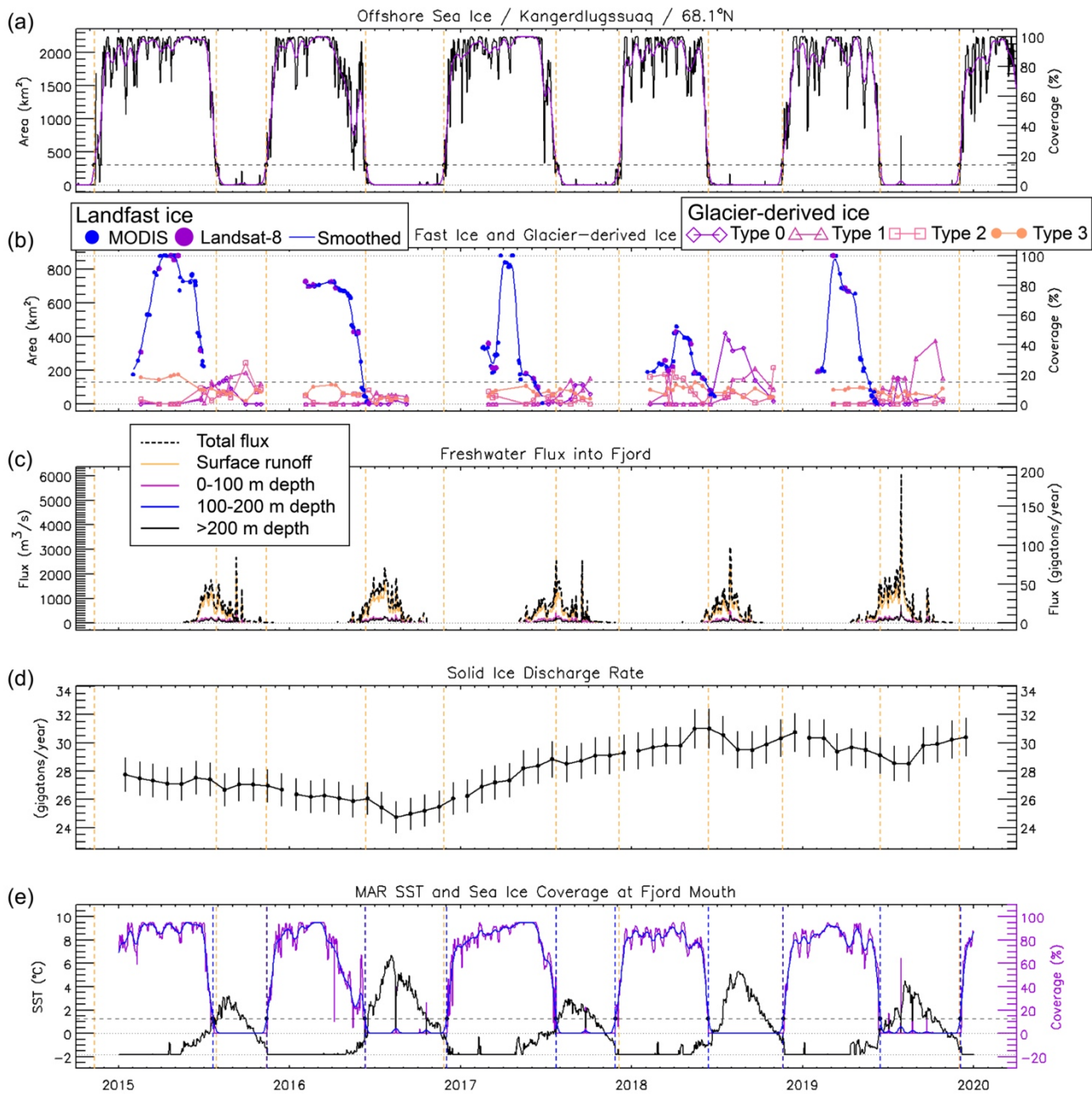
Figure A3. Time series for fjord 18 (Kangerdlussuaq) showing: a) daily (black line) sea-ice area (km²) and percent coverage based on AMSR2 sea ice concentration, along with a 31-day running mean (purple), b) area (km²) and percent coverage for fast ice evaluated from MODIS (blue dot) and Landsat (purple dot) single image sources and with smoothed (blue) record and for all four surface character types (0-3) for glacier-derived ice, c) total freshwater flux (m³ s⁻¹, black dashed line) and depth-binned (solid line) freshwater flux, d) cumulative fjord solid ice discharge (Gt yr⁻¹), and e) sea surface temperature (black line) and sea ice coverage (purple line) measured at the fjord mouth from MAR climate data. Vertical dashed orange lines in all panels indicate the freeze-up and break-up dates for offshore sea ice (panel a) as measured by passing a threshold of 15% of mean March-April sea ice area. A similar threshold is indicated (dashed line) in panel e, while panel b is a simple 15% threshold (dashed line). The 15% threshold is indicated by a dashed line in panels a, b, and e.

446
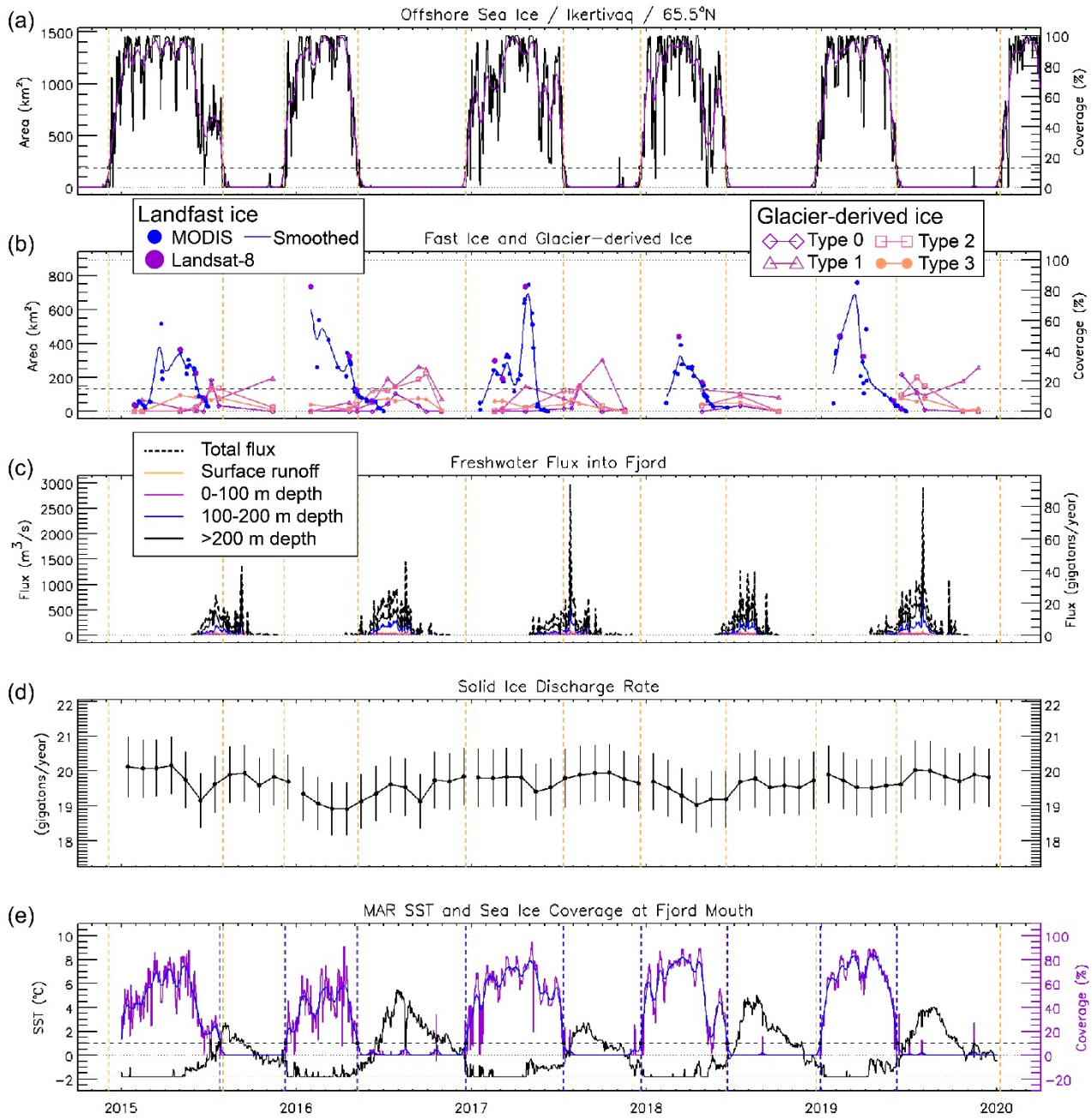
447
448 **Figure A4. Same as Fig. A3 for fjord 31 (Ikertivaq).**
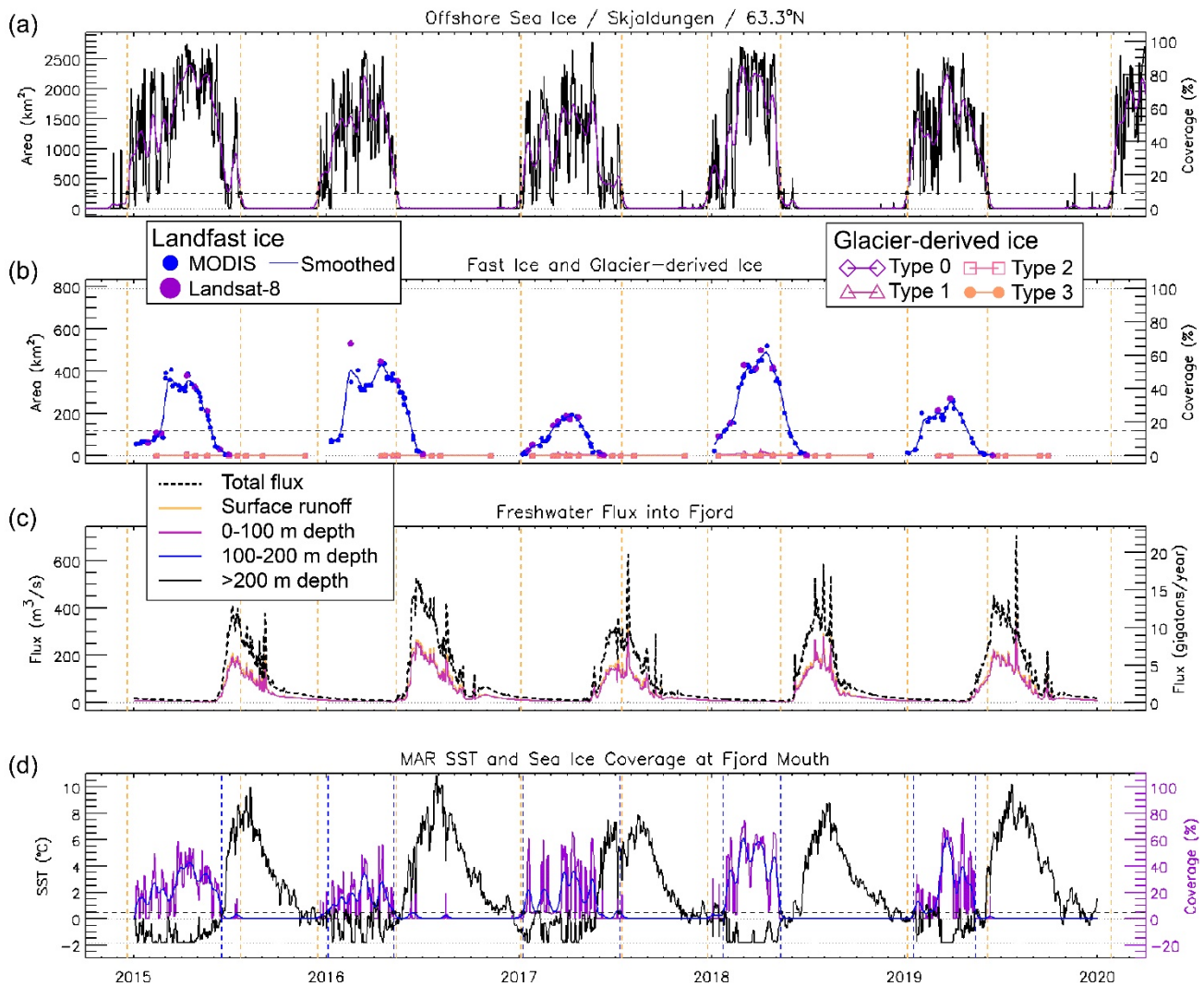
449
450 **Figure A5. Same as Fig. A3 for fjord 37 (Skjoldungen), but with no solid ice discharge data and panel (e) presented as panel (d).**
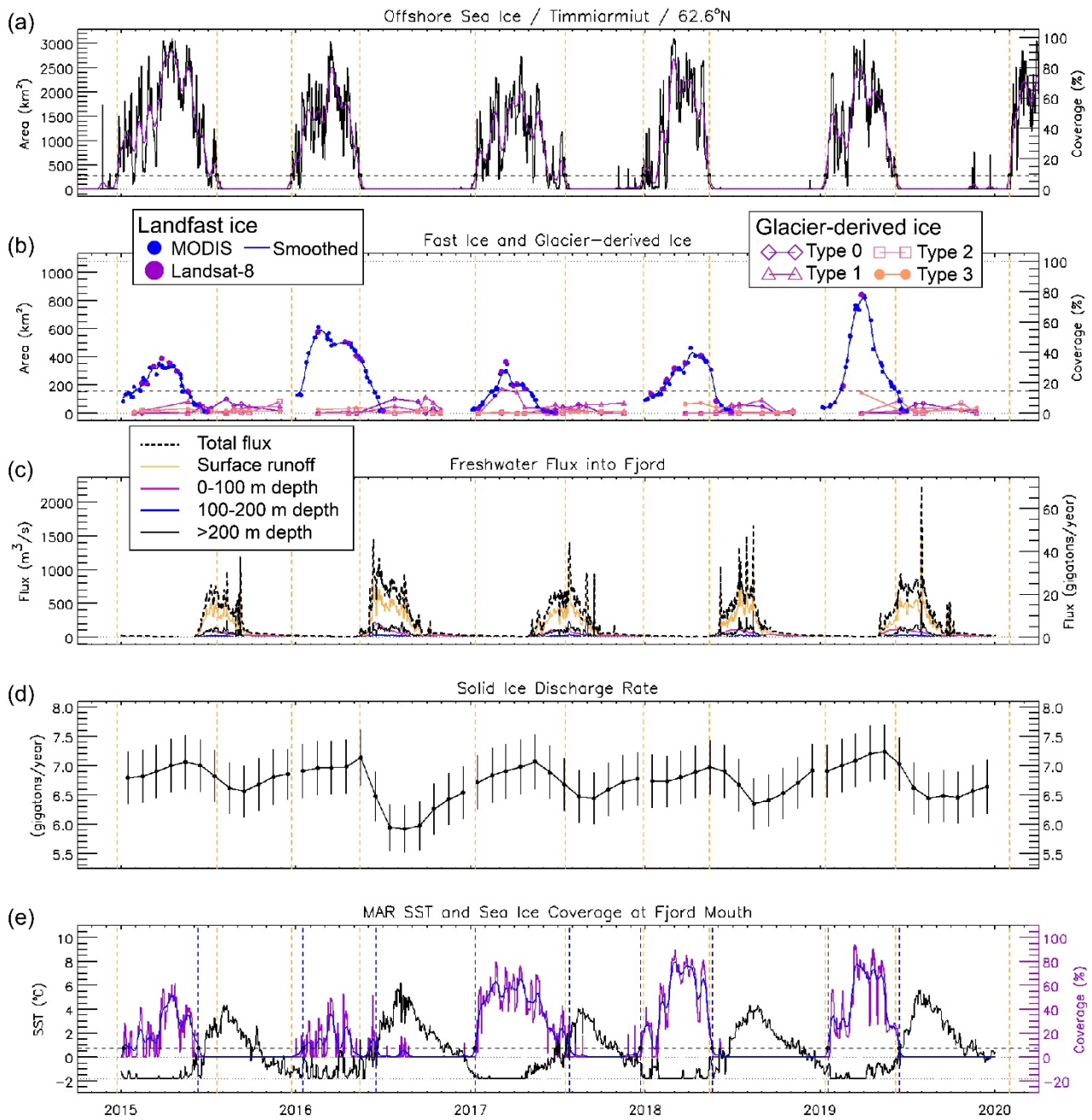
Figure A6. Same as Fig. A3 for fjord 40 (Timmiarmiut).
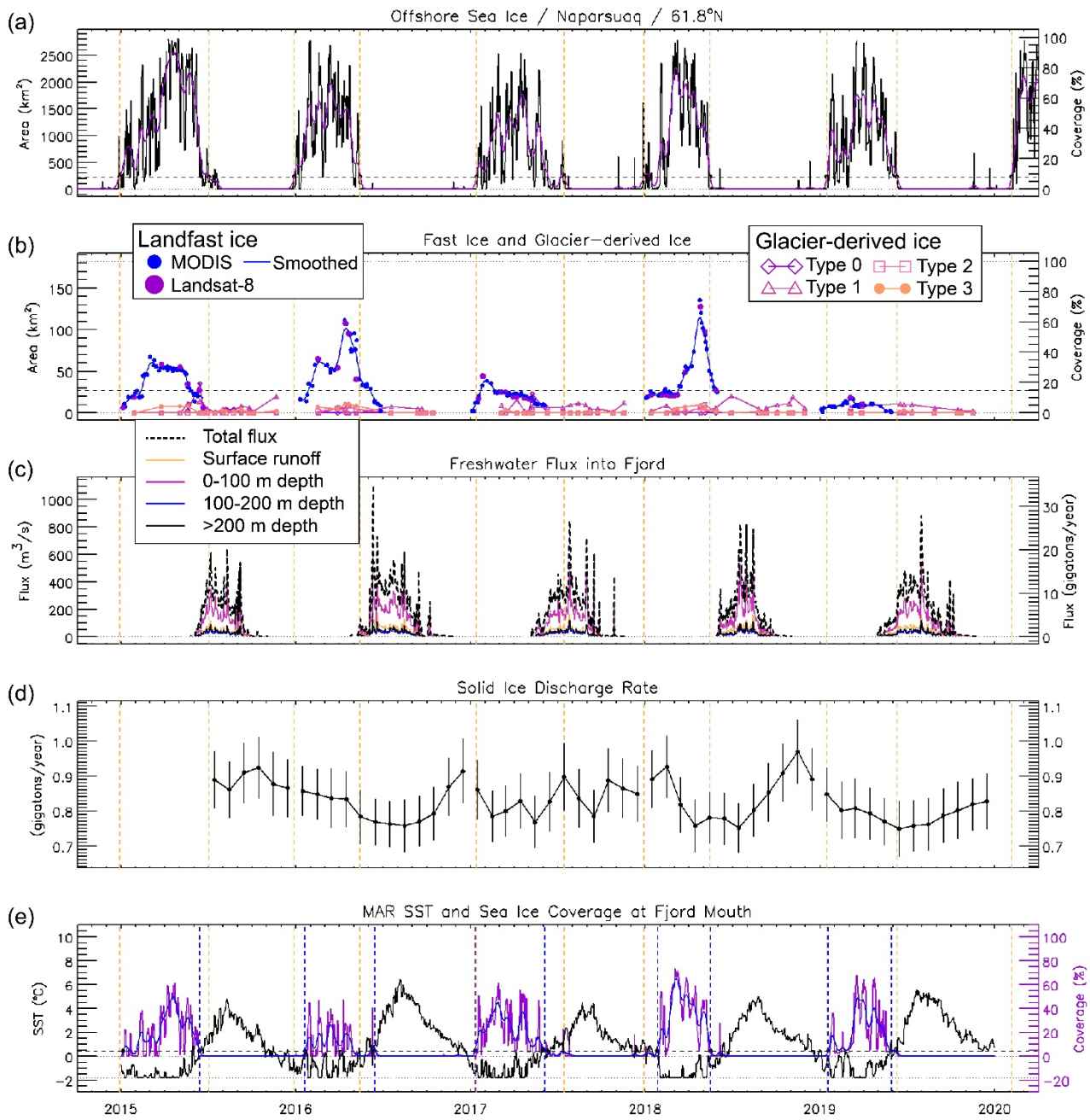
454
455   **Figure A7. Same as Fig. A3 for fjord 43 (Naparsuaq).**
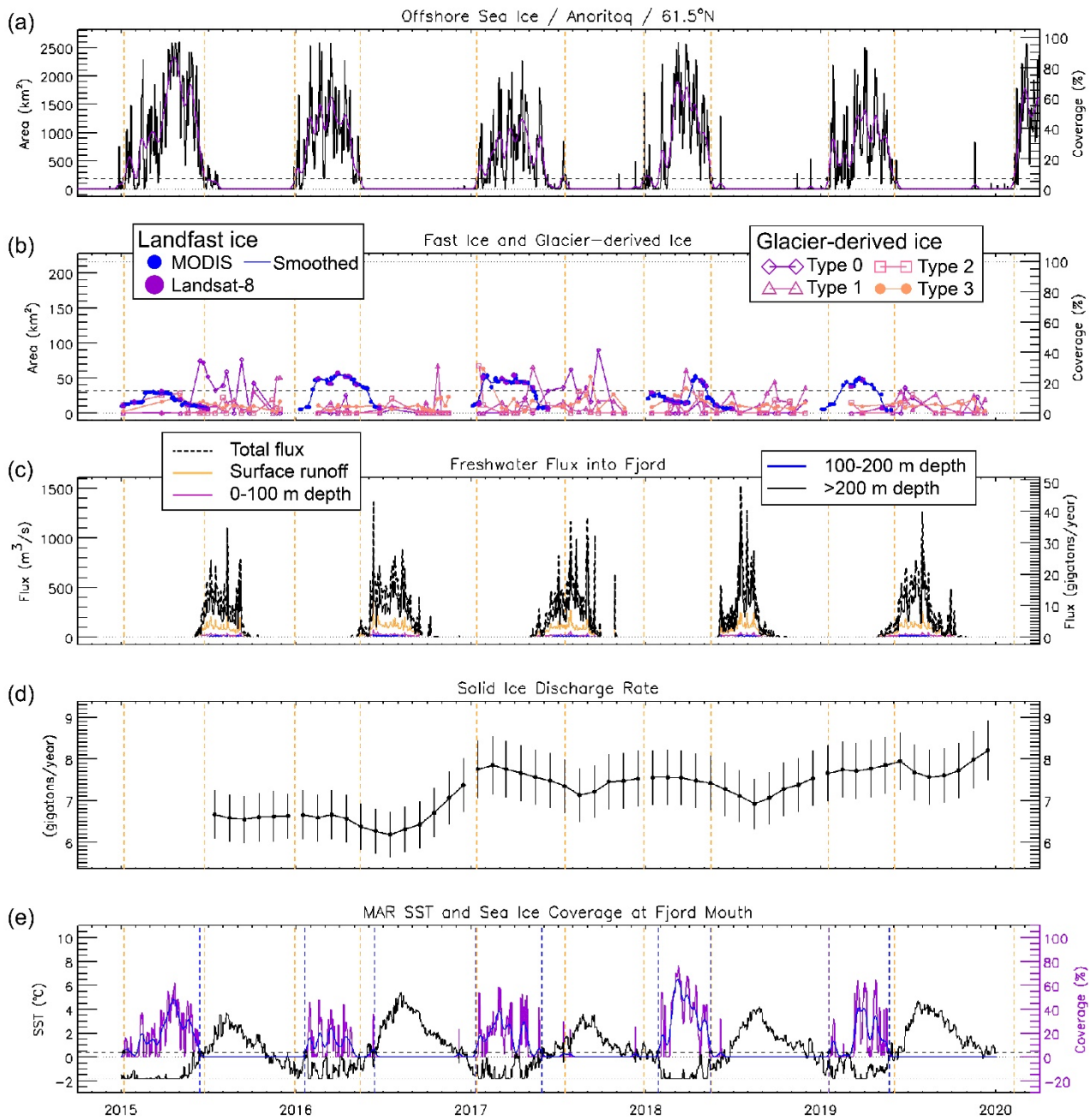
Figure A8. Same as Fig. A3 for fjord 45 (Anoritoq).
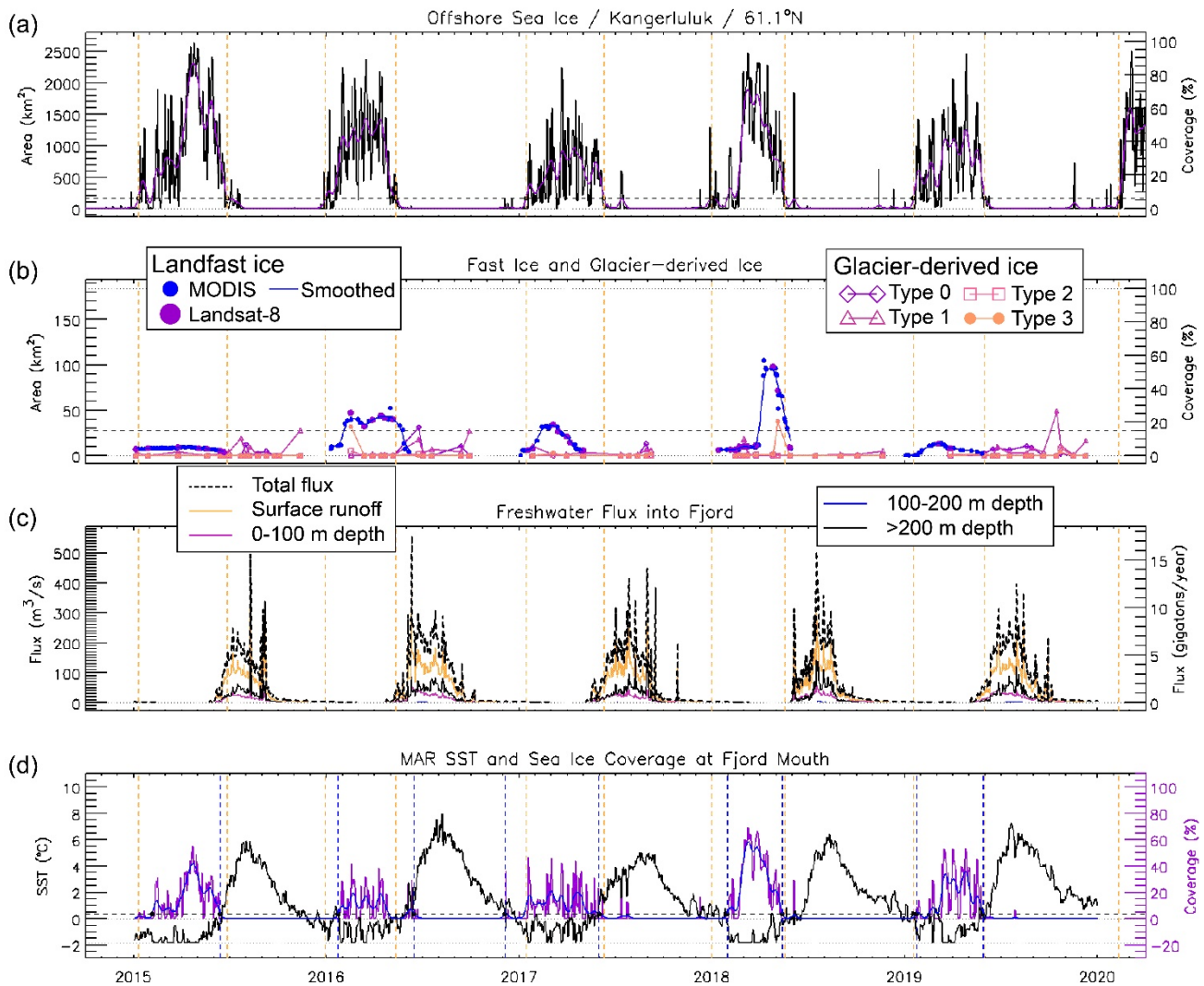
458
459 **Figure A9. Same as Fig. A3 for fjord 48 (Kangerluluk), but with no solid ice discharge data and panel (e) presented as panel (d).**

460

461

462

463

464

465

466

467

Table A1. Statistics for landfast ice in SEG focus fjords. Using a threshold of 15% areal coverage to define the landfast ice season, each table entry contains the start day (day-of-year, doy), end day (doy), and duration (days) of the landfast ice season. Landfast ice analysis did not span the full 12-month year and < symbol indicates likely earlier presence while the > symbol indicates likely later/longer presence. Years when the landfast ice coverage never exceeded the 15% threshold are marked as ---. The last two columns give the mean and standard deviation of the start day (doy), end day (doy), and duration (days). Standard deviation is not calculated for records of likely longer length (> or < included). Dates are based on use of smoothed data (see section 3.3).

		2015	2016	2017	2018	2019	Mean	Stdv
Nansen	Start day (doy)	<42	<34	<47	<65	<30	<43.6	
	End day (doy)	>179	>159	175	148	144	>161.1	
	Duration (days)	>137	>125	>128	>83	>114	>117.5	
Kangerdlugssuaq		<32	<35	<47	<34	<31	<35.8	
		>182	157	158	158	142	>159.3	
		>150	>122	>111	>124	>111	>123.4	
Ikertivaq		65	<31	34	50	<25	<40.8	
		160	124	137	119	116	131.1	18.0
		95	>93	103	69	>91	>90.2	
Skjoldungen		52	28	62	25	31	39.6	16.3
		148	163	124	148	120	140.4	18.3
		96	135	62	123	89	100.8	28.8
Timmiarmiut		30	11	52	35	43	34.0	15.5
		134	164	120	145	159	144.3	18.0
		104	153	68	110	116	110.3	30.4
Naparsuaq		43	27	22	70	---	40.3	21.6
		147	156	52	151	---	126.4	50.1
		104	129	30	81	---	86.1	42.2
Anoritoq		---	36	21	94	42	48.4	31.8
		---	148	130	127	117	130.4	13.3
		---	112	109	33	75	81.9	37.2
Kangerluluk		---	34	43	89	---	55.3	29.5
		---	143	76	144	---	120.8	39.0
		---	109	33	55	---	65.6	38.7

Code and data availability

Data created to support this research is archived at the National Snow and Ice Data Center (Cohen et al., 2023).

The code for freshwater and solid ice discharge data analysis and visualization is available at

https://github.com/tarynblack/southeast_greenland_fjords [*This will be formally archived as a repository with DOI before final publication*].

481 Solid ice discharge data: v79 published 2023-05-05 at https://doi.org/10.22008/promice/data/ice_discharge/d/v02

482 Freshwater discharge data: v4.2 published 2022-08-28 at https://doi.org/10.22008/FK2/XKQVL7

483 **Author contributions and competing interests**

484 We used the CRediT taxonomy (https://casrai.org/credit/) to evaluate individuals' contributions and order authorship. All

485 authors designed the study and contributed to the writing and editing of the manuscript. TM and KL administrated the project

486 with TM supervising this research component. BC, TB, and HS were responsible for data collection and formal analyses. TM,

487 BC, TB, and HS validated data and produced data visualizations. IJ advised regarding early research methods.

488 The authors declare that they have no conflicts of interest.

489 **Acknowledgements**

490 This research was supported via NASA Biological Diversity and Ecological Forecasting Programs and Cryospheric Sciences

491 (NNX11AO63G, NNX13AN28G, 80NSSC18K1229, and 80NSSC20K1361). We acknowledge Xavier Fettweis for

492 assistance with MAR regional climate model data and Brice Noël for assistance with RACMO regional climate model data

493 (included in some archived code and data but not within manuscript results). We also acknowledge Ken Mankoff for

494 assistance and consultation on use and interpretation of solid ice discharge and freshwater flux datasets.

495 **References**

496 Aschwanden, A., Fahnestock, M. A., Truffer, M., Brinkerhoff, D. J., Hock, R., Khroulev, C., Mottram, R., and Khan, S. A.:

497 Contribution of the Greenland Ice Sheet to sea level over the next millennium, Sci. Adv., 5, eaav9396,

498 https://doi.org/10.1126/sciadv.aav9396, 2019.

499 Beitsch, A., Kaleschke, L. and Kern, S.: Investigating High-Resolution AMSR2 Sea Ice Concentrations during the February

500 2013 Fracture Event in the Beaufort Sea, Rem. Sens., 6, 3841-3856, https://doi.org/10.3390/rs6053841, 2014.

501 Bochow, N., Poltronieri, A., Robinson, A., Montoya, M., Rypdal, M., and Boers, N.: Overshooting the critical threshold for

502 the Greenland ice sheet, Nature, 622, 528–536, https://doi.org/10.1038/s41586-023-06503-9, 2023.

503 Bosson, J. B., Huss, M., Cauvy-Fraunié, S., Clément, J. C., Costes, G., Fischer, M., Poulenard, J., and Arthaud, F.: Future

504 emergence of new ecosystems caused by glacial retreat, Nature, 620, 562–569, https://doi.org/10.1038/s41586-023-06302-2,

505 2023.

Cohen, B., Black, T., and Moon, T.: Southeast Greenland Fjord Physical Characteristics for 2015-2019, Boulder, Colorado USA, NASA National Snow and Ice Data Center Distributed Active Archive Center, https://doi.org/10.5067/R86BW8LR6PZH, 2023. (*Under Review*)

Enderlin, E. M., Carrigan, C. J., Kochtitzky, W. H., Cuadros, A., Moon, T., and Hamilton, G. S.: Greenland iceberg melt variability from high-resolution satellite observations, The Cryosphere, 12, 565–575, https://doi.org/10.5194/tc-12-565-2018, 2018.

Fettweis, X., Box, J. E., Agosta, C., Amory, C., Kittel, C., Lang, C., As, D. V., Machguth, H., and Gallée, H.: Reconstructions of the 1900–2015 Greenland ice sheet surface mass balance using the regional climate MAR model, The Cryosphere, 11, 1015–1033, https://doi.org/10.5194/tc-11-1015-2017, 2017.

Fox-Kemper, B., Hewitt, H.T., Xiao, C., Aðalgeirsdóttir, G., Drijfhout, S.S., Edwards, T.L., Golledge, N.R., Hemer, M., Kopp, R.E., Krinner, G., Mix, A., Notz, D., Nowicki, S., Nurhati, I.S., Ruiz, L., Sallée, J.-B., Slangen, A.B.A., and Yu, Y.: Ocean, Cryosphere and Sea Level Change, in: Climate Change 2021: The Physical Science Basis. Contribution of Working Group I to the Sixth Assessment Report of the Intergovernmental Panel on Climate Change, edited by: Masson-Delmotte, V., Zhai, P., Pirani, A., Connors, S.L., Péan, C., Berger, S., Caud, N., Chen, Y., Goldfarb, L., Gomis, M.I., Huang, M., Leitzell, K., Lonnoy, E., Matthews, J.B.R., Maycock, T.K., Waterfield, T., Yelekçi, O., Yu, R., and Zhou, B., Cambridge University Press, Cambridge, United Kingdom and New York, NY, USA, 1211–1362, doi:10.1017/9781009157896.011, 2021.

Gallagher, M. R., Shupe, M. D., Chepfer, H., and L'Ecuyer, T.: Relating snowfall observations to Greenland ice sheet mass changes: an atmospheric circulation perspective, The Cryosphere, 16, 435–450, https://doi.org/10.5194/tc-16-435-2022, 2021.

Gelderloos, R., Haine, T. W. N., and Almansi, M.: Subinertial Variability in Four Southeast Greenland Fjords in Realistic Numerical Simulations, J. Geophys. Res.: Oceans, 127, https://doi.org/10.1029/2022jc018820, 2022.

Heide-Jørgensen, M. P., Chambault, P., Jansen, T., Gjelstrup, C. V. B., Rosing-Asvid, A., Macrander, A., Víkingsson, G., Zhang, X., Andresen, C. S., and MacKenzie, B. R.: A regime shift in the Southeast Greenland marine ecosystem, Global Change Biol, https://doi.org/10.1111/gcb.16494, 2022.

Hersbach, H., Bell, B., Berrisford, P., Hirahara, S., Horányi, A., Muñoz-Sabater, J., Nicolas, J., Peubey, C., Radu, R., Schepers, D., Simmons, A., Soci, C., Abdalla, S., Abellan, X., Balsamo, G., Bechtold, P., Biavati, G., Bidlot, J., Bonavita, M., Chiara, G., Dahlgren, P., Dee, D., Diamantakis, M., Dragani, R., Flemming, J., Forbes, R., Fuentes, M., Geer, A., Haimberger, L., Healy, S., Hogan, R. J., Hólm, E., Janisková, M., Keeley, S., Laloyaux, P., Lopez, P., Lupu, C., Radnoti, G., Rosnay, P., Rozum, I., Vamborg, F., Villaume, S., and Thépaut, J.: The ERA5 global reanalysis, Q. J. R. Meteorol. Soc., 146, 1999–2049, https://doi.org/10.1002/qj.3803, 2020.

Holding, J. M., Markager, S., Juul-Pedersen, T., Paulsen, M. L., Møller, E. F., Meire, L., and Sejr, M. K.: Seasonal and spatial patterns of primary production in a high-latitude fjord affected by Greenland Ice Sheet run-off, Biogeosciences, https://doi.org/10.5194/bg-16-3777-2019, 2019.

Hopwood, M. J., Carroll, D., Browning, T. J., Meire, L., Mortensen, J., Krisch, S., and Achterberg, E. P.: Non-linear response of summertime marine productivity to increased meltwater discharge around Greenland, Nat. Commun., https://doi.org/10.1038/s41467-018-05488-8, 2018.

Hopwood, M. J., Carroll, D., Dunse, T., Hodson, A., Holding, J. M., Iriarte, J. L., Ribeiro, S., Achterberg, E. P., Cantoni, C., Carlson, D. F., Chierici, M., Clarke, J. S., Cozzi, S., Fransson, A., Juul-Pedersen, T., Winding, M. H. S., and Meire, L.: Review article: How does glacier discharge affect marine biogeochemistry and primary production in the Arctic?, The Cryosphere, 14, 1347–1383, https://doi.org/10.5194/tc-14-1347-2020, 2020.

Kaleschke, L. and Tian-Kunze, X.: AMSR2 ASI 3.125 km Sea Ice Concentration Data, V0.1, Institute of Oceanography, University of Hamburg, Germany, digital media (ftp-projects.zmaw.de/seaice/), 2016.

Karlsson, N. B., Mankoff, K. D., Solgaard, A. M., Larsen, S. H., How, P. R., Fausto, R. S., and Sørensen, L. S.: A data set of monthly freshwater fluxes from the Greenland ice sheet's marine-terminating glaciers on a glacier–basin scale 2010–2020, GEUS Bulletin, 53, https://doi.org/10.34194/geusb.v53.8338, 2023.

Karlsson, N. B., Solgaard, A. M., Mankoff, K. D., Gillet-Chaulet, F., MacGregor, J. A., Box, J. E., Citterio, M., Colgan, W. T., Larsen, S. H., Kjeldsen, K. K., Korsgaard, N. J., Benn, D. I., Hewitt, I. J., and Fausto, R. S.: A first constraint on basal melt-water production of the Greenland ice sheet, Nat. Commun., 12, 3461, https://doi.org/10.1038/s41467-021-23739-z, 2021.

Kelly, B. P., Bengtson, J. L., Boveng, P. L., Cameron, M. F., Dahle, S. P., Jansen, J. K., Logerwell, E. A., Overland, J. E., Sabine, C. L., Waring, G. T., and Wilder, J. M.: Status review of the ringed seal (Phoca hispida), U.S. Dep. Commer., NOAA Tech. Memo. NMFS-AFSC-212, 250 p, 2010.

Kim, Y.-H., Min, S.-K., Gillett, N. P., Notz, D., and Malinina, E.: Observationally-constrained projections of an ice-free Arctic even under a low emission scenario, Nat. Commun., 14, 3139, https://doi.org/10.1038/s41467-023-38511-8, 2023.

Kochtitzky, W. and Copland, L.: Retreat of Northern Hemisphere Marine-Terminating Glaciers, 2000–2020, Geophys. Res. Lett., 49, https://doi.org/10.1029/2021GL096501, 2022.

Laidre, K. L. and Stirling, I.: Grounded icebergs as maternity denning habitat for polar bears (Ursus maritimus) in North and Northeast Greenland, Polar Biology, 43, 937–943, https://doi.org/10.1007/s00300-020-02695-2, 2020.

Laidre, K. L., Supple, M. A., Born, E. W., Regehr, E. V., Wiig, Ø., Ugarte, F., Aars, J., Dietz, R., Sonne, C., Hegelund, P., Isaksen, C., Akse, G. B., Cohen, B., Stern, H. L., Moon, T., Vollmers, C., Corbett-Detig, R., Paetkau, D., and Shapiro, B.: Glacial ice supports a distinct and undocumented polar bear subpopulation persisting in late 21st-century sea-ice conditions, Science, 376, 1333–1338, https://doi.org/10.1126/science.abk2793, 2022.

Lenaerts, J. T. M., Medley, B., Broeke, M. R., and Wouters, B.: Observing and Modeling Ice Sheet Surface Mass Balance, Rev. Geophys., 57, 376–420, https://doi.org/10.1029/2018rg000622, 2019.

Mahoney, A. R., Eicken, H., Gaylord, A. G., and Gens, R.: Landfast sea ice extent in the Chukchi and Beaufort Seas: The annual cycle and decadal variability, Cold Reg. Sci. Technol., 103, 41–56, https://doi.org/10.1016/j.coldregions.2014.03.003, 2014.

Mankoff, K.: Greenland freshwater runoff, GEUS Dataverse, V2, https://doi.org/10.22008/FK2/AA6MTB, 2020.

Mankoff, K. D., Noël, B., Fettweis, X., Ahlstrøm, A. P., Colgan, W., Kondo, K., Langley, K., Sugiyama, S., van As, D., and Fausto, R. S.: Greenland liquid water discharge from 1958 through 2019, Earth Syst. Sci. Data, 12, 2811–2841, https://doi.org/10.5194/essd-12-2811-2020, 2020a.

Mankoff, K. D.; Solgaard, A., Larsen, S.: Greenland Ice Sheet solid ice discharge from 1986 through last month: Discharge, GEUS Dataverse, V54, https://doi.org/10.22008/promice/data/ice_discharge/d/v02, 2020b.

Mankoff, K. D., Solgaard, A., Colgan, W., Ahlstrøm, A. P., Khan, S. A., and Fausto, R. S.: Greenland Ice Sheet solid ice discharge from 1986 through March 2020, Earth Syst. Sci. Data, 12, 1367–1383, https://doi.org/10.5194/essd-12-1367-2020, 2020c.

McGovern, M., Poste, A. E., Oug, E., Renaud, P. E., and Trannum, H. C.: Riverine impacts on benthic biodiversity and functional traits: A comparison of two sub-Arctic fjords, Estuar., Coast. and Shelf Sci., 240, https://doi.org/10.1016/j.ecss.2020.106774, 2020.

Meire, L., Paulsen, M. L., Meire, P., Rysgaard, S., Hopwood, M. J., Sejr, M. K., Stuart-Lee, A., Sabbe, K., Stock, W., and Mortensen, J.: Glacier retreat alters downstream fjord ecosystem structure and function in Greenland, Nat. Geosci., 16, 671–674, https://doi.org/10.1038/s41561-023-01218-y, 2023.

Moon, T. A., Gardner, A. S., Csatho, B., Parmuzin, I., and Fahnestock, M. A.: Rapid reconfiguration of the Greenland Ice Sheet coastal margin, J. Geophys. Res.: Earth Surf., 125, e2020JF005585, https://doi.org/10.1029/2020jf005585, 2020.

Moon, T. A., Mankoff, K. D., Fausto, R. S., Fettweis, X., Loomis, B. D., Mote, T. L., Poinar, K., Tedesco, M., Wehrlé, A., and Jensen, C. D.: Greenland Ice Sheet, in: Arctic Report Card 2022, edited by: Druckenmiller, M. L., Thoman, R. L., and Moon, T. A., https://doi.org/10.25923/c430-hb50, 2022.

Moon, T., Sutherland, D. A., Carroll, D., Felikson, D., Kehrl, L., and Straneo, F.: Subsurface iceberg melt key to Greenland fjord freshwater budget, Nat. Geosci., 11, 49–54, https://doi.org/10.1038/s41561-017-0018-z, 2017.

Morlighem, M., Williams, C. N., Rignot, E., An, L., Arndt, J. E., Bamber, J. L., Catania, G., Chauché, N., Dowdeswell, J. A., Dorschel, B., Fenty, I., Hogan, K., Howat, I., Hubbard, A., Jakobsson, M., Jordan, T. M., Kjeldsen, K. K., Millan, R., Mayer, L., Mouginot, J., Noël, B. P. Y., O'Cofaigh, C., Palmer, S., Rysgaard, S., Seroussi, H., Siegert, M. J., Slabon, P., Straneo, F., Broeke, M. R. V. D., Weinrebe, W., Wood, M., and Zinglersen, K. B.: BedMachine v3: Complete bed topography and ocean bathymetry mapping of Greenland from multibeam echo sounding combined with mass conservation., Geophysical Research Letters, 44, 11051–11061, https://doi.org/10.1002/2017gl074954, 2017.

Morlighem, M. et al.: IceBridge BedMachine Greenland, Version 5 [Data Set], Boulder, Colorado USA. NASA National Snow and Ice Data Center Distributed Active Archive Center, https://doi.org/10.5067/GMEVBWFLWA7X, date accessed 11-02-2023, 2022.

Murray, C., Markager, S., Stedmon, C. A., Juul-Pedersen, T., Sejr, M. K., and Bruhn, A.: The influence of glacial melt water on bio-optical properties in two contrasting Greenlandic fjords, Estuarine, Coastal and Shelf Science, 163(PB), 72–83, https://doi.org/10.1016/j.ecss.2015.05.041, 2015.

Noël, B., Berg, W. J. van de, Lhermitte, S., and van den Broeke, M. R.: Rapid ablation zone expansion amplifies north Greenland mass loss, Sci. Adv., 5, https://doi.org/10.1126/sciadv.aaw0123, 2019.

Petrich, C., Eicken, H., Zhang, J., Krieger, J., Fukamachi, Y., and Ohshima, K. I.: Coastal landfast sea ice decay and breakup in northern Alaska: Key processes and seasonal prediction, J. Geophys. Res., 117, C02003, https://doi.org/10.1029/2011jc007339, 2012.

Rastner, P., Bolch, T., Mölg, N., Machguth, H., Bris, R. L., and Paul, F.: The first complete inventory of the local glaciers and ice caps on Greenland, The Cryosphere, 6, 1483–1495, https://doi.org/10.5194/tc-6-1483-2012, 2012.

Scheick, J., Enderlin, E. M., and Hamilton, G.: Semi-automated open water iceberg detection from Landsat applied to Disko Bay, West Greenland, J. Glaciology, 65, 468–480, https://doi.org/10.1017/jog.2019.23, 2019.

Sejr, M. K., Bruhn, A., Dalsgaard, T., Juul-Pedersen, T., Stedmon, C. A., Blicher, M., Meire, L., Mankoff, K. D., and Thyrring, J.: Glacial meltwater determines the balance between autotrophic and heterotrophic processes in a Greenland fjord, Proc. Nat. Acad. Sci., 119(52), e2207024119, https://doi.org/10.1073/pnas.2207024119, 2022.

Soldal, I., Dierking, W., Korosov, A., and Marino, A.: Automatic Detection of Small Icebergs in Fast Ice Using Satellite Wide-Swath SAR Images, Remote Sensing, 11, 806–24, https://doi.org/10.3390/rs11070806, 2019.

Stern, H. L. and Laidre, K. L.: Sea-ice indicators of polar bear habitat, The Cryosphere, 10, 2027–2041, https://doi.org/10.5194/tc-10-2027-2016, 2016.

627 van As, D., Hasholt, B., Ahlstrøm, A. P., Box, J. E., Cappelen, J., Colgan, W., Fausto, R. S., Mernild, S. H., Mikkelsen, A.
628 B., Noël, B. P. Y., Petersen, D. and van den Broeke, M. R.: Reconstructing Greenland Ice Sheet meltwater discharge
629 through the Watson River (1949–2017), Arc., Ant., and Alpine Res., 50:1, https://doi.org/10.1080/15230430.2018.1433799,
630 2018.

631 van Dongen, E. C. H., Jouvet, G., Sugiyama, S., Podolskiy, E. A., Funk, M., Benn, D. I., Lindner, F., Bauder, A., Seguinot,
632 J., Leinss, S., and Walter, F.: Thinning leads to calving-style changes at Bowdoin Glacier, Greenland, The Cryosphere, 15,
633 485–500, https://doi.org/10.5194/tc-15-485-2021, 2021.

634 White, D.R.: Propagation of Uncertainty and Comparison of Interpolation Schemes, Int J Thermophys 38, 39,
635 https://doi.org/10.1007/s10765-016-2174-6, 2017.